Chapter 5
Mafic Lower-Mantle Mineral Association

Abstract Mafic mineral association in the lower mantle is subordinate to the ultramafic one. It includes bridgmanite, CaSi-perovskite, SiO_2 and anhydrous aluminous phases. The former three are the same as that observed in the ultramafic association; but their chemical compositions differ from those in the ultramafic association, mainly in the significant enrichment of Al. Among aluminous phases the NAL phase occurs at low-pressure conditions and is replaced by a CF phase at a depth of 800–1200 km depth. NAL phase is also concentrated in Na and K, while CF phase does not contain K. The partition coefficient of aluminium between bridgmanite and the NAL phase vary from 0.10 to 0.26, demonstrating that the Al enrichment in bridgmanite occurs at the expense of the Al decrease in the NAL phases. The Al concentration in the CF phase remains constant and the Al concentration in bridgmanite, after reaching maximal concentrations (24–25 wt%) with disintegration of the NAL phase, remains constant as well. In addition to the major minerals, phase Egg, δ-AlOOH, and a series of dense hydrous magnesium silicates (DHMS) are expected to be present in the mafic association. Among these DHMS, Phase D and Phase H are most likely to occur in the subducting slabs within the lower mantle. Some of these minerals (phase Egg and δ-AlOOH) are observed in natural geological materials; the others have only been synthesized in laboratory experiments.

5.1 General

Mafic association in the lower mantle appears as a consequence of recrystallization from subducting slab materials, predominantly of the middle-ocean ridge basalt (MORB) composition during the course of the subduction of lithospheric plates through the 660 km discontinuity. MORB contains more silica (48–51 wt% SiO_2) and aluminium (15–16 wt% Al_2O_3) than the bulk mantle, and therefore is composed of a different mineral association than the juvenile ultramafic composition. Four major mineral phases complete the mafic mineral association in the lower mantle: bridgmanite, CaSi-perovskite, SiO_2, and anhydrous aluminous phase (NAL, CF and/or CAS) (Funamori et al. 2000; Hirose et al. 2005; Akaogi 2007; Ricolleau et al.

F.V. Kaminsky, *The Earth's Lower Mantle*, Springer Geology,
DOI 10.1007/978-3-319-55684-0_5

2010). The first three minerals above are the same as those observed in the ultramafic association; they experienced similar phase transformations with pressure. However, the mafic association is not as commonly observed as the ultramafic counterparts; only a few samples have been identified as inclusions in lower-mantle diamond to date (Wirth et al. 2007; Walter et al. 2011; Thomson et al. 2014).

The chemical compositions of the mafic association, established from high pressure–temperature (*P–T*) experiments on MORB materials, differ from those in the ultramafic association, mainly in the significant enrichment in Al (Kesson et al. 1994; Hirose et al. 1999, 2005; Ono et al. 2001; Hirose and Fei 2002; Litasov et al. 2004; Litasov and Ohtani 2005; Ricolleau et al. 2010). In addition to the major mineral phases mentioned above, high *P–T* experimental results have showed the occurrence of various minor hydrous minerals at relevant *P–T* conditions of the subducting slabs, such as hydrous aluminium phases (Phase Egg and δ-AlOOH) and a series of DHMS. Phase Egg and δ-AlOOH have been observed in geological environments, but other hydrous minerals are known only from experiments and theoretical calculations.

5.2 Major Minerals

5.2.1 Bridgmanite

According to high-pressure experiments with dry MORB compositions, the occurrence of bridgmanite is associated with CaSi-perovskite, stishovite and Al-rich phase(s) at 27–80 GPa. It has a significantly lower magnesium index *mg* = 0.567–0.771 (average 0.658 ± 0.124), higher concentration of Al (Al_2O_3 = 11.1–24.0 wt %; average 16.23 ± 4.15 wt%), as well as higher concentrations of Ti and Ca than low-Al bridgmanite from the ultramafic association with an average *mg* = 0.916 and Al_2O_3 = 1.55 wt% (Kesson et al. 1994; Hirose et al. 1999, 2005; Ono et al. 2001; Hirose and Fei 2002; Litasov et al. 2004; Litasov and Ohtani 2005; Ricolleau et al. 2010) (Table 5.1; Fig. 5.1). Experimental synthesis of bridgmanite using a hydrated mafic composition at 25–28 GPa and ~1500 °C shows that bridgmanite has a similar composition with *mg* = 0.630 and may be associated with Al-rich Phase D (Litasov and Ohtani 2005; Pamato et al. 2015).

Bridgmanite from the natural mafic association identified in Juina-5 kimberlite pipe, Brazil, has similar compositions with *fe* = 0.346–0.401 and Al_2O_3 = 16.26–18.37 wt% (Table 5.1) (Thomson et al. 2014).

The concentration of Al in bridgmanite of the mafic association depends on the pressure at which it forms. The Al concentration is doubled from 11 to 13 wt% Al_2O_3 at 26 GPa to 24 wt% Al_2O_3 at 100 GPa, while the *mg* value remains almost constant (Fig. 5.2). Considering this correlation as a possible geobarometer, natural 'mafic' bridgmanite from Juina-5 pipe with 16.26–18.37 wt% Al_2O_3 have been formed at ~65–75 GPa. Such a drastic increase of wt% Al_2O_3 with pressure is most likely correlated to the redistribution of Al in bridgmanite from an Al-rich phase with increasing pressure. On the other hand, while Ca and Na concentrations in bridgmanite show a positive correlation with Al concentration (Fig. 5.3a,b) that is similar to that in

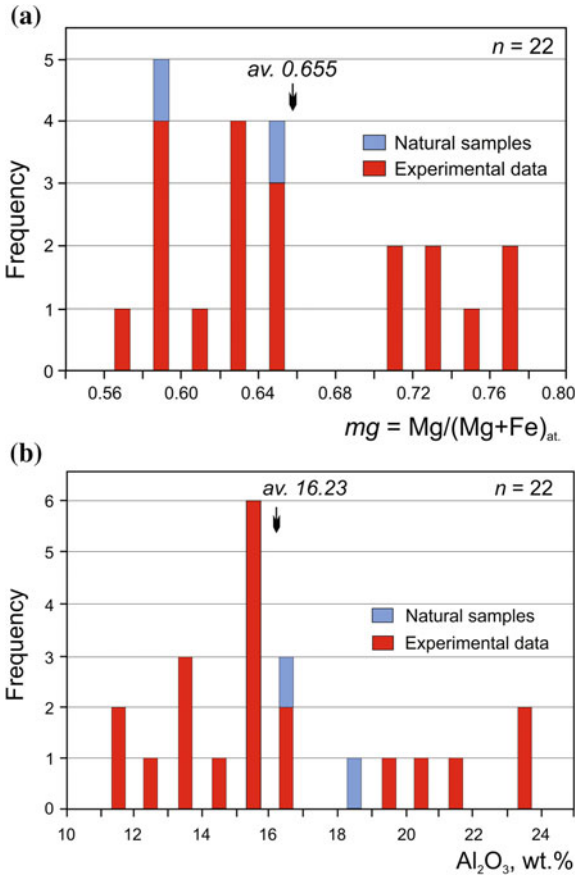

Fig. 5.1 Distribution of *mg* index (**a**) and Al_2O_3 (**b**) in bridgmanite from the mafic association. Data from Kesson et al. (1994), Hirose et al. (1999, 2005), Ono et al. (2001), Hirose and Fei (2002), Litasov et al. (2004), Litasov and Ohtani (2005), Ricolleau et al. (2010), Thomson et al. (2014)

bridgmanite of the ultramafic association, the correlation of Al with iron index *fe* is negative (Fig. 5.3c). That is, the most Al-rich bridgmanite are more Mg-rich.

Among bridgmanite varieties of the ultramafic association, there is also a group with a high Al concentration (see Sect. 4.2.2). However, those high-Al 'ultramafic' bridgmanite samples, in comparison with bridgmanite from the mafic association, are significantly richer in Mg, Ca, Na and Cr (0.64–5.32 wt% against 0.02–1.19 wt % CaO; 0.82–6.21 wt% against 0–0.11 wt% Na_2O; 1.19–3.14 wt% against 0.04–0.45 wt% Cr_2O_3, respectively) (Fig. 5.3).

Table 5.1 Representative compositions of bridgmanite synthesised from MORB materials at high pressures and temperatures and from natural samples (wt%)

Starting material	Synthetic MORB glass			Fresh natural MORB		Synthetic MORB glass		Juina-5 pipe, Brazil	
P (Gpa)	29.2	28	28	44	55	80	100	N/A	N/A
T (K)	1943	1873	1873	2391	2550	N/A	N/A	N/A	N/A
Sample No.	mbk-2	K-244dry	K-244wet	MORB#4	MORB#5			Ju5-31a	Ju5-117b
Mineral association	Brd + CaSiPrv + Sti + CF	Brd + CaSiPrv + Sti + NAL		Brd + CaSiPrv + Sti + NAL + CF	Brd + CaSiPrv + Sti + CF			Brd	Brd
SiO_2	41.5	38.6	35.2	42.3	40.9	43.0	44.7	35.64	36.14
TiO_2	3.27	4.38	5.12	2.5	2.1	n.a.	n.a.	5.48	3.77
Al_2O_3	11.4	13.4	15.3	21.2	23.6	20.5	24.0	16.26	18.37
Cr_2O_3	n.a.	n.a.	n.a.	n.a.	n.a.	n.a.	n.a.	0.05	0.04
FeO	21.0	21.2	23.2	11.3	10.1	13.9	11.7	21.79	18.39
MnO	n.a.	n.a.	n.a.	n.a.	n.a.	n.a.	n.a.	0.68	0.56
MgO	20.3	20.2	19.3	18.7	19.1	20.2	15.9	18.24	19.45
CaO	1.13	0.57	0.51	3.5	3.3	0.6	1.4	0.12	0.11
Na_2O	0.74	0.35	0.39	0.5	0.8	1.9	2.2	0.11	0.16
K_2O	0.02	0.01	0.01	n.a.	n.a.	n.a.	n.a.	0.01	0.00
Total	99.4	98.7	99.0	100.0	99.9	100.1	99.9	98.38	97.00
fe	0.367	0.370	0.403	0.253	0.229	0.278	0.292	0.401	0.346
mg	0.633	0.630	0.597	0.747	0.771	0.722	0.708	0.599	0.654
Reference	Litasov et al. (2004)	Litasov and Ohtani (2005)		Ricolleau et al. (2010)		Kesson et al. (1994)		Thomson et al. (2014)	

Note n.a. not analysed

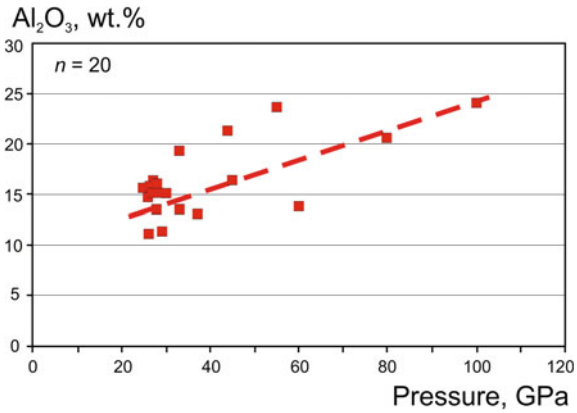

Fig. 5.2 Al_2O_3 concentration as a function of pressure in bridgmanite synthesised using MORB compositions at high pressures and temperatures. Data from Kesson et al. (1994), Hirose et al. (1999, 2005), Ono et al. (2001), Hirose and Fei (2002), Litasov et al. (2004), Litasov and Ohtani (2005), Ricolleau et al. (2010)

5.2.2 *$CaSiO_3$*

Representative chemical compositions of CaSi-perovskite from experimental studies on mafic associations are shown in Table 5.2. Similar to the compositions of bridgmanite discussed above, it is enriched in Al: 0.89–4.49 wt% Al_2O_3 (average: 2.49 wt%) as compared with the Al concentration of 0.1–1.52 wt% (average: 0.29 wt%) in CaSi-perovskite from the ultramafic association (Fig. 5.4a). The Al concentration in CaSi-perovskite synthesized from MORB materials remains almost constant within the entire pressure range of 25–113 GPa where the mineral was synthesized. CaSi-perovskite from natural association identified in Juina-5 pipe (Brazil), by contrast, has very low concentrations of Al_2O_3 (0.14–0.20 wt%; Thomson et al. 2014), similar to concentrations of Al_2O_3 in CaSi-perovskite from the ultramafic association (see Figs. 4.21 and 5.4b).

Although Fe and Mg concentrations in CaSi-perovskite from the mafic association are significantly higher than in the ultramafic association, the magnesium indices in CaSi-perovskites from the both associations are similar (averages: 0.519 and 0.521, respectively) (Fig. 5.4b).

There are, among natural CaSi-perovskite from the mafic association, high-Ti varieties with TiO_2 = 6.64–23.09 wt% TiO_2 (Thomson et al. 2014). Similar to the ultramafic association, $Ca(Si,Ti)O_3$ grains have dissolution structures (Fig. 4e in Thomson et al. 2014).

Concentrations of Fe, Mg and minor elements, such as Na, are significantly greater in CaSi-perovskite from the mafic association in comparison to this mineral from the ultramafic association (Fig. 5.5). Fe and Mg show positive correlation with Al.

The Al-concentration in $CaSiO_3$ is found to influence the transition boundary of the tetragonal to cubic structure transition, increasing it from 550 to 1900 K at

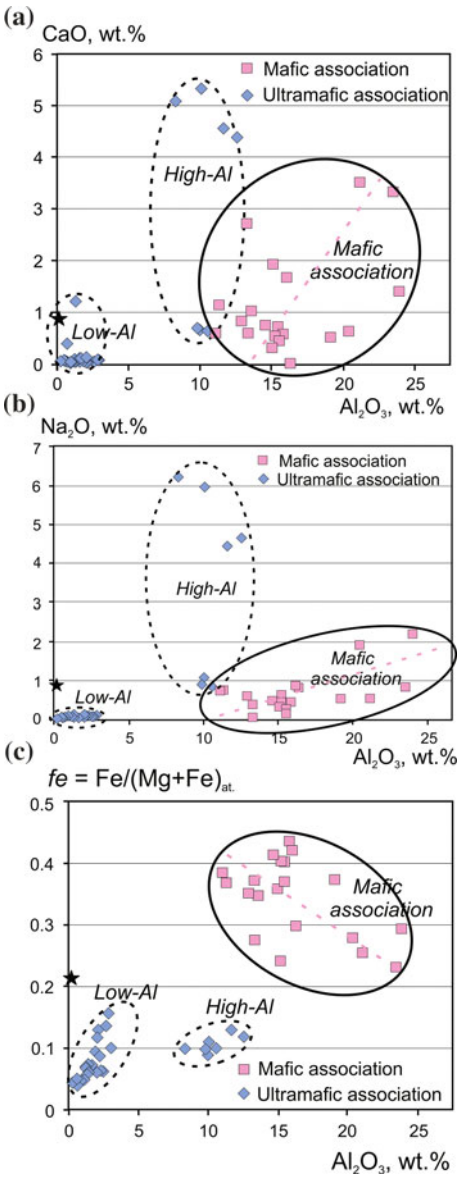

Fig. 5.3 Chemical characteristics of bridgmanite from the mafic association (n = 20) in comparison to bridgmanite from the ultramafic association (n = 34). **a** CaO versus Al_2O_3. **b** Na_2O versus Al_2O_3. **c** Iron index fe versus Al_2O_3. Data from Kesson et al. (1994), Hutchison (1997), Hirose et al. (1999, 2005), Stachel et al. (2000), Kaminsky et al. (2001), Ono et al. (2001), Hirose and Fei (2002), Davies et al. (2004), Litasov et al. (2004), Hayman et al. (2005), Litasov and Ohtani (2005), Tappert et al. (2009), Ricolleau et al. (2010), Zedgenizov et al. (2014, 2015). Star shows the composition of bridgmanite from the Tenham meteorite after Tschauner et al. (2014)

60 GPa with increasing Al_2O_3 concentration from 0 to 5.9 wt% (Kurashina et al. 2004). The tetragonal → cubic transition may thus occur in relatively cold subducted lithospheric slabs where $CaSiO_3$ perovskite can contain a higher proportion of Al_2O_3 (Hirose et al. 2005).

Table 5.2 Representative compositions of CaSi-perovskite synthesized from MORB materials and from natural samples (wt%)

Starting material	Synthetic MORB glass			Fresh natural MORB		Synthetic MORB glass		Juina-5 pipe, Brazil	
P (Gpa)	29.2	28	28	44	55	80	100	N/A	N/A
T (K)	1943	1873	1873	2391	2550	N/A	N/A	N/A	N/A
Sample No.	mbk-2	K-244wet	K-244dry	MORB#4	MORB#5			Ju5-52	Ju5-82
Mineral association	Brd + CaSiPrv + Sti + CF			Brd + CaSiPrv + Sti + NAL + CF	Brd + CaSiPrv + Sti + CF			CaSiPrv + ZrO_2	Ca(Si,Ti) Prv
SiO_2	47.9	48.9	49.3	51.9	52.1	56.7	55.0	51.27	37.48
TiO_2	2.22	2.71	2.58	1.3	1.2	n.a.	n.a.	0.02	23.09
Al_2O_3	4.06	1.64	2.08	3.5	2.5	2.1	2.2	0.14	2.93
FeO	5.13	0.97	1.46	4.4	3.5	2.6	1.6	0.24	0.14
MnO	n.a.	n.a.	n.a.	n.a.	n.a.	n.a.	n.a.	0.06	0.00
MgO	3.10	0.61	0.71	3.2	3.9	1.4	0.9	0.05	0.00
CaO	36.4	44.4	43.3	35.7	36.8	36.7	39.2	47.38	28.74
Na_2O	0.75	0.31	0.32	0.1	0.1	<0.5	1.2	0.16	0.06
K_2O	0.17	0.04	0.06	n.a.	n.a.	n.a.	n.a.	0.11	0.02
Total	99.7	99.6	99.8	100.1	100.1	99.5	100.1	99.43	93.80
fe	0.481	0.471	0.535	0.435	0.335	0.510	0.499	0.729	1.000
mg	0.519	0.529	0.465	0.565	0.665	0.490	0.501	0.271	0.000
Reference	Litasov et al. (2004)	Litasov and Ohtani (2005)		Ricolleau et al. (2010)		Kesson et al. (1994)		Thomson et al. (2014)	

Note n.a. not analysed

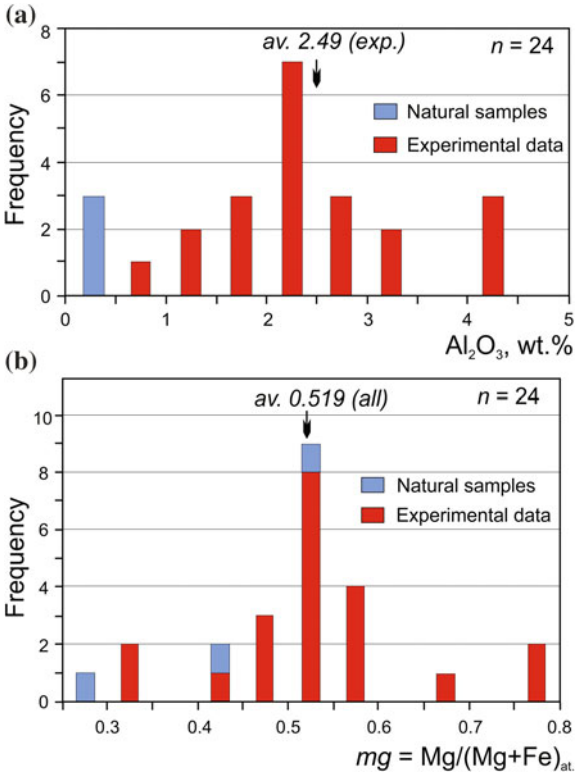

Fig. 5.4 Distribution of Al_2O_3 (**a**) and *mg* index (**b**) in CaSi-perovskite from the mafic association. Data from Kesson et al. (1994), Hirose et al. (1999, 2005), Ono et al. (2001), Hirose and Fei (2002), Litasov et al. (2004), Litasov and Ohtani (2005), Ricolleau et al. (2010)

5.2.3 SiO_2

SiO_2 from the mafic association is synthesized within a range of 25–100 GPa and, like perovskitic minerals, also has an elevated Al concentration: 0.35–4.2 wt% Al_2O_3 with an average of 2.59 wt% Al_2O_3; 10.3 wt% Al_2O_3 as was reported for one case (Table 4.3). It increases up to 12.6 wt% at 113 GPa in seifertite (Hirose et al. 2005). The only known natural sample of SiO_2 from the mafic association in Juina-5 pipe, Brazil, does not have high Al_2O_3 (0.09 wt%; Thomson et al. 2014). This may be caused by its association with kyanite, which is probably formed as a result of dissociation and collecting the entire amount of Al from the initial high-pressure composition.

Stishovite reported in experimental works under pressure values of 80–100 GPa (Kesson et al. 1994) is doubtful because at such *P*–*T* conditions $CaCl_2$-structured SiO_2 is stable. Moreover, experiments by Hirose et al. (2005) with MORB compositions demonstrated that the phase transition boundary between Al-bearing stishovite and $CaCl_2$-structured SiO_2 is lower than that of pure SiO_2 by ~25 GPa: it is located at ~62 GPa under 2000 K, which corresponds to a depth of ~1500 km (Table 5.3).

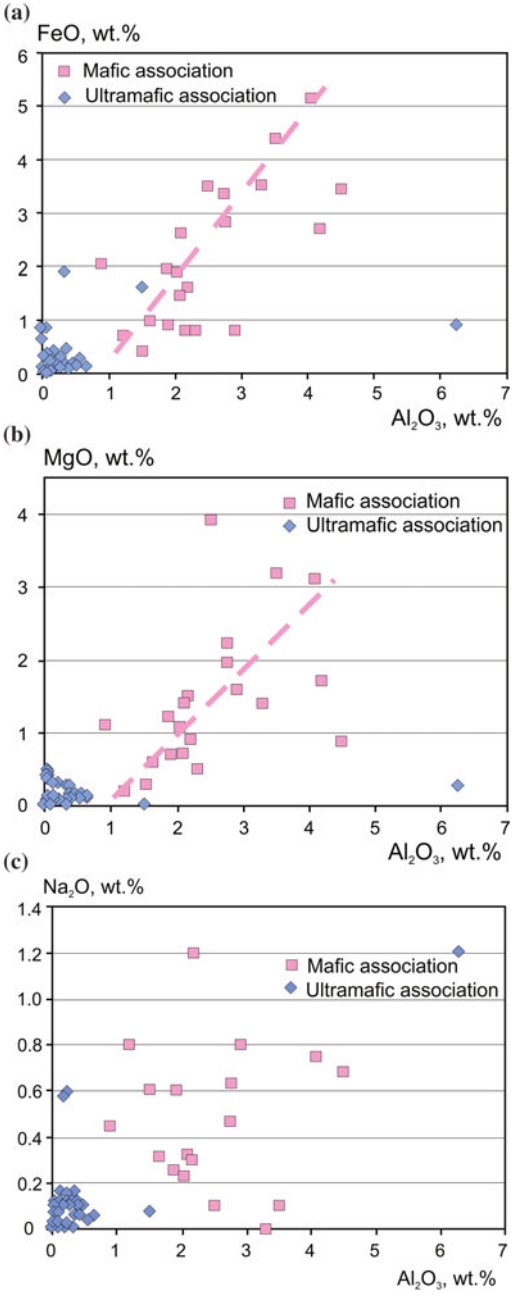

Fig. 5.5 Chemical characteristics of CaSi-perovskite from the mafic association. **a** *fe* versus Al_2O_3; **b** *mg* versus Al_2O_3; **c** Na versus Al_2O_3

Table 5.3 Representative compositions of SiO_2 from experimental and natural mafic associations (wt%)

Starting material	Synthetic MORB glass			Fresh natural MORB		Synthetic MORB glass		Juina-5 pipe, Brazil
P (Gpa)	29.2	28	28	44	55	80	100	N/A
T (K)	1943	1873	1873	2391	2550	N/A	N/A	N/A
Sample No.	mbk-2	K-244wet	K-244dry	MORB#4	MORB#5			Ju5-90
Mineral association	Brd + CaSiPrv + Sti + CF			Brd + CaSiPrv + Sti + NAL + CF		Brd + CaSiPrv + Sti + CF		SiO_2 + Ky
SiO_2	98.5	96.5	96.4	98.7	98.5	88.5	96.1	100.07
TiO_2	n.a.	0.01	0.04	0.1	0.1	n.a.	n.a.	0.03
Al_2O_3	1.15	3.04	2.41	0.8	0.9	10.3	2.7	0.09
FeO	0.14	0.13	0.23	0.1	0.1	<0.5	<0.5	0.01
NiO	n.a.	n.a.	n.a.	n.a.	n.a.	n.a.	n.a.	0.02
MgO	n.a.	0.08	0.09	0	0.1	<0.5	<0.5	0.01
CaO	n.a.	0.06	0.05	0.1	0.4	<0.5	<0.5	0.02
Na_2O	0.34	0.04	0.03	0.0	0.0	<0.5	<0.5	0.03
Total	100.1	99.9	99.3	99.8	100.1	98.8	98.8	100.29
Reference	Litasov et al. (2004)	Litasov and Ohtani (2005)		Ricolleau et al. (2010)		Kesson et al. (1994)		Thomson et al. (2014)

Note n.a. not analysed

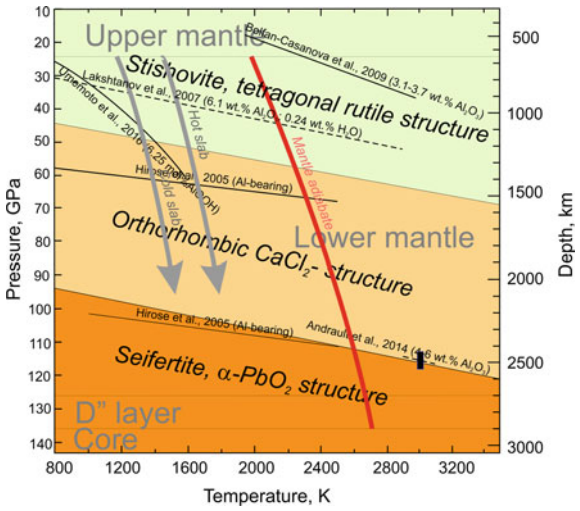

Fig. 5.6 Phase diagram for SiO_2 in subducted slabs. Temperature profiles in slabs after Kirby et al. (1996). Data from Hirose et al. (2005), Lakshtanov et al. (2007), Bolfan-Casanova et al. (2009), Andrault et al. (2014), and Umemoto et al. (2016). Mantle adiabate after Katsura et al. (2010)

Concentration of H_2O in stishovite has been shown to be related to the Al admixture in silica. While Al-free stishovite contains only 16–30 wt. ppm H_2O, synthetic stishovite with 4.4 wt% Al_2O_3 contains ~3010 wt. ppm H_2O (Litasov et al. 2007a). Most hydrogen in stishovite is associated with Al^{3+} substitutional defects on the octahedral (Si^{4+}) site. The hydrogen can occupy 40% of vacancies created by the incorporation of Al^{3+} at 20 GPa (Litasov et al. 2007a). It is possible that Al actually forms an AlOOH phase with H_2O, which is highly soluble in stishovite (e.g., Chung and Kagi 2002; Panero and Stixrude 2004). The incorporation of Al and H_2O into SiO_2 significantly reduces the transition pressure for the stishovite to post-stishovite transition boundary (Fig. 5.6). Specifically, hydrous Al-bearing stishovite transforms to post-stishovite at 24 GPa and 298 K, which is far lower than the transition pressure of 50–60 GPa for pure silica (Lakshtanov et al. 2007). First-principles static calculations and molecular dynamics demonstrated that hydrogen bonds and hydrogen mobility play a crucial role in lowering the post-stishovite transition pressure (Umemoto et al. 2016). A co-operative redistribution of hydrogen atoms is the main mechanism responsible for the reduction of the transition pressure in hydrous Al-bearing stishovite. Stishovite, containing 6.25 mol% AlOOH, transforms into $CaCl_2$-structured phase at pressures from 30 to 32 GPa (1000 K) to 50 GPa (1300 K), i.e., within the range of 800–1200 km depth. Since SiO_2 is a candidate composition in the subducted slabs, it can undergo a series of the aforementioned phase transitions that are influenced by their Al concentrations, causing stratification in the subducting slabs in the lower mantle: at 1200–1300 km depth with stishovite → $CaCl_2$-structure transition and at 2200–2300 km with $CaCl_2$-structure → seifertite transition (Fig. 5.6). This is similar to the stratification in juvenile ultramafic mantle, except for the presence of the aluminous mineral phase. In addition, phase boundaries in subducted slabs are located higher compared with the juvenile ultramafic host.

5.3 Anhydrous Aluminous Phases

5.3.1 General

High *P–T* experiments on anhydrous oceanic basalts have demonstrated that an aluminous phase with the calcium–ferrite (CF) structure (space group *Pbnm*, $Z = 4$) appears at pressures above 25 GPa and with temperatures above 1200 °C (Irifune and Ringwood 1993; Kesson et al. 1994; Ono 2001). The CF phase occurs in association with bridgmanite, CaSi-perovskite and SiO_2 at high *P–T*. Subsequently, another aluminous phase, named a 'new hexagonal aluminous phase' (NAL), which has a similar chemical composition to the CF phase, was observed in the garnet-to-perovskite transformation in the $MgAl_2O_4$–$CaAl_2O_4$ system at relevant conditions of the lower mantle (Akaogi et al. 1999; Miyajima et al. 1999, 2001). The NAL and CF phases can comprise 10–30% of the subducted MORB materials in the lower mantle (Ricolleau et al. 2010; Mookherjee et al. 2012).

Studies of diamonds from the Juina-5 kimberlite in Brazil indicated that their mineral inclusions have compositions consistent with the phase assemblage expected to crystallize from basaltic materials at lower-mantle conditions: bridgmanite, CaSi-perovskite, SiO_2, and NAL and CF phases (Walter et al. 2011). These results provide geological evidence for the possible existence of the NAL and CF phases in the lower mantle.

5.3.2 New Hexagonal Aluminous Phase (NAL)

The NAL phase has a general formula of $^{IX}A^{VIII}B_2^{VI}C_6O_{12}$, where ^{IX}A sites are comprised by large monovalent or divalent cations (Na^+, K^+ and/or Ca^{2+}), ^{VIII}B sites are represented by smaller cations (Mg^{2+} and Fe^{2+}), and ^{VI}C octahedral sites are occupied by Al^{3+} (mostly), Si^{4+} and Fe^3. The full chemical formula of NAL is $(Na, K, Ca)(Mg, Fe^{2+})_2(Al, Fe^{3+}, Si)_6O_{12}$. Both Na- and K-rich NAL phases were synthesized at pressures of 22–25 GPa and a temperature of 1500 °C (Kojitani et al. 2011). Hence, the NAL phase concentrates not only Al but also alkalis, while the CF phase does not accommodate potassium (Miyajima et al. 2001; Guignot and Andrault 2004).

Representative compositions of NAL are shown in Table 5.4. Concentrations of both Na (4.93–5.9 wt% Na_2O; average 5.46 wt%) and K (0.54–1.94 wt% K_2O; average 1.00 wt%) are quite constant, and are independent of other components and pressure conditions. Al_2O_3 has a strong linear negative correlation with SiO_2, demonstrating their substitution in the C site (Fig. 5.7a). The Al/Si_{at} strongly decreases from 4.7 at 25 GPa to 1.73 at 33 GPa (Fig. 5.7b), which coincides with the increase of the Al concentration with increasing pressure in the associated bridgmanite.

Table 5.4 Representative compositions of the NAL phase from experimental mafic associations (wt%)

Starting material	Synthetic MORB glass					Fresh natural MORB	
P (Gpa)	25	26	28	28	28	33	44
T (K)	1273	1773	1873	1873	2573		
Sample No.	K-156	K-206wet	K-244wet	K-244dry	K-254	MORB#1	MORB#2
Mineral association	Brd + CaSiPrv + Sti + NAL						
Brd + CaSiPrv + Sti + NAL + CF							
SiO_2	13.5	15.0	15.9	20.2	22.4	26.5	23.3
TiO_2	0.40	1.21	1.11	1.06	1.14	0.3	0.3
Al_2O_3	53.8	52.1	51.0	47.3	44.2	38.9	45.0
FeO	11.9	11.7	11.4	12.4	11.4	8.7	4.7
MgO	12.6	11.9	12.2	10.7	12.6	17.7	18.9
CaO	1.16	1.39	1.80	1.60	2.01	2.2	1.9
Na_2O	5.79	5.67	5.40	5.68	5.12	5.9	5.9
K_2O	0.72	0.79	0.89	0.54	0.96	n.a.	n.a.
Total	99.9	99.8	99.7	99.5	99.8	100.2	100.0
fe	0.346	0.355	0.344	0.394	0.336	0.216	0.122
mg	0.654	0.645	0.656	0.606	0.664	0.784	0.878
Al/Si (at.)	4.698	4.094	3.781	2.760	2.326	1.730	2.277
Reference	Litasov and Ohtani (2005)					Ricolleau et al. (2010)	

Note n.a. not analysed

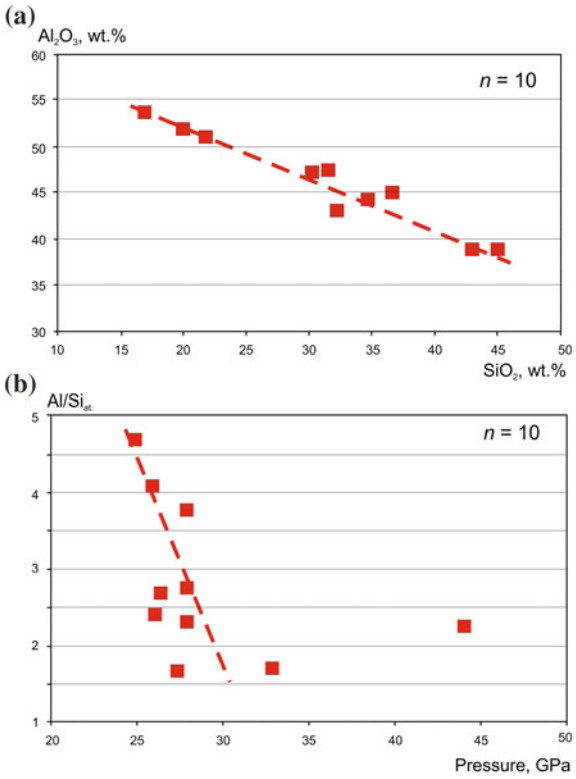

Fig. 5.7 Chemical characteristics of the NAL phase. **a** Al_2O_3 versus SiO_2. **b** Al/Si versus pressure. Data from Hirose and Fei (2002), Litasov et al. (2004), Litasov and Ohtani (2005), Ricolleau et al. (2010)

The NAL phase has a hexagonal crystal structure with the space group of $P6_3/m$ (Gasparik et al. 2000; Miura et al. 2000; Miyajima et al. 2001; Kojitani et al. 2011; Mookherjee et al. 2012; Wicks and Duffy 2016; Wu et al. 2016a) (Fig. 5.8). The ^{IX}A site is a nine-fold coordinated tunnel with a hexagonal cross-section and is occupied by a large monovalent (Na^+, K^+) or divalent cation (Ca^{2+}). Cations in the ^{IX}A site are likely to be disordered owing to its Wyckoff symmetry being 2*a* and the fact that only one atom occupies either of the two equivalent sites, i.e., there is half occupancy (Mookherjee et al. 2012). The B site is six-fold co-ordinated but trigonal prismatic rather than octahedral and is typically occupied by Mg^{2+} (or replacing with Fe^{2+} in a Fe-rich variety). Each Mg^{2+} ion is surrounded by three double chains of AlO_6 (SiO_6) octahedra connected by corner-sharing oxygen ions. They form the C site. Large channels are formed by these octahedra in three double chains and are occupied typically by Na^+ or K^+ ions at half occupancy. The distorted C octahedra form edge-sharing double chains extending along the *c* axis that are corner linked to form tunnels. Within the tunnels lie the larger A sites while the smaller B sites are

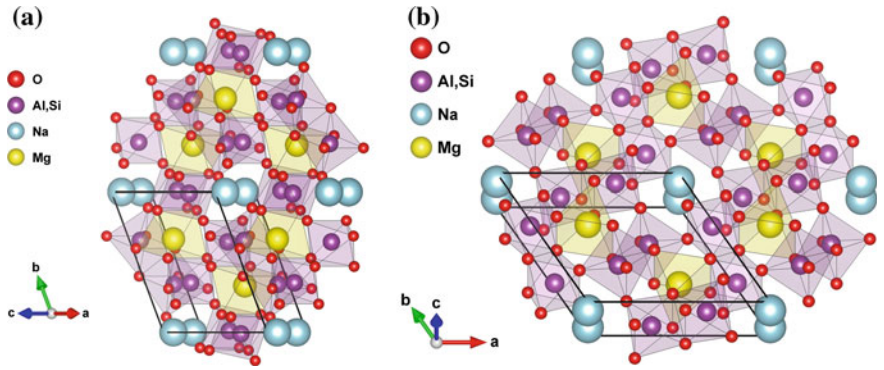

Fig. 5.8 Hexagonal crystal structure of Fe-free NAL (space group $P6_3/m$) in different axis orientations. Lattice parameters from Pamato et al. (2014)

surrounded by three double chains. With multiple sites that can each accept more than one cation, the NAL structure can accommodate a wide range of compositional variation. The large cation sites in the NAL structure allow them to be potential hosts for the alkali elements (Wicks and Duffy 2016).

The hexagonal NAL structure is stable under pressure conditions of up to 40–50 GPa, after which it transforms to the orthorhombic CF phase (Ono et al. 2009; Ricolleau et al. 2010; Imada et al. 2011) in accordance with the later theoretical results obtained using the first-principles computational method (Kawai and Tsuchiya 2012). The enrichment of the NAL phase in potassium significantly increases its stability up to 141 GPa (Guignot and Andrault 2004; Kato et al. 2013).

Density functional theory calculations showed that the NAL phase has lower seismic velocities compared with the CF phase, and NAL could contribute to low-velocity provinces in the deep mantle (Mookherjee et al. 2012). However, calculations performed by Kawai and Tsuchiya (2012) concluded that NAL and CF phases would have comparable shear wave velocities, producing less than 1% velocity difference across the phase transition; this conclusion is in agreement with experiments carried out by Pamato et al. (2014).

Since the NAL phase probably contains up to 12 mol% of iron (Litasov and Ohtani 2005; Ricolleau et al. 2010; see Table 5.4), the valence and spin states of iron in the NAL phase can potentially affect its elasticity, which in turn can affect our understanding of the mineral physics of the MORB assemblage in the lower mantle (Lin et al. 2013; Wu et al. 2016b). Recently, two single-crystal samples (iron-free $Na_{1.14}Mg_{1.83}Al_{4.74}Si_{1.23}O_{12}$ and iron-bearing $Na_{0.71}Mg_{2.05}Al_{4.62}Si_{1.16}Fe^{2+}_{0.09}Fe^{3+}_{0.17}O_{12}$) were studied by Wu et al. (2016a) using synchrotron nuclear forward scattering (NFS) and X-ray diffraction (XRD) combined with diamond-anvil cells (DACs) up to 86 GPa at room temperature to investigate the potential effects of the spin transition on its equation of state at high pressures. Based on the evaluation of the hyperfine quadrupole splitting from NFS results, a pressure-induced high-spin (HS) to low-spin (LS) transition of the octahedral Fe^{3+} in the iron-bearing NAL was observed

at approximately 30 GPa. Compared with the equation of state for the iron-free NAL phase using XRD data, the iron-bearing NAL undergoes a volume reduction of 1.0% (~ 1.2 Å^3) at 33–47 GPa, which is associated with the spin transition of the octahedral Fe^{3+}. The bulk sound velocities (V_Φ) of the iron-free and iron-bearing NAL phase are approximately 6% larger than those of Al, Fe-bearing bridgmanite and CaSi-perovskite in the lower mantle, except for the spin transition region where a notable softening of V_Φ with a maximum reduction of 9.4% occurs in the iron-bearing NAL phase at 41 GPa. Considering the high volume proportion of the NAL phase in subducted MORB, the distinct elastic properties of the iron-bearing NAL phase across the spin transition may provide an explanation for the observed seismic heterogeneities of subducted slabs in the lower mantle at depths below 1200 km.

5.3.3 *Aluminous Phase with the Calcium–Ferrite Structure (CF Phase)*

The CF phase, which is considered as a high-pressure modification of NAL, has a general formula on a 12 oxygen basis to make it better comparable with the NAL phase, of $^{VIII}B_3^{VI}C_6O_{12}$, where ^{VIII}B sites are occupied by Na^+, Ca^{2+} and Mg^{2+} cations and the ^{VI}C sites are framework-forming cations Al^{3+} (mostly) and Si^{4+}, similar to that in the NAL phase. However, unlike the NAL phase, it is significantly enriched (almost doubled) in sodium (average 10.55 wt% Na_2O) and does not contain potassium. Its full chemical formula is $(Na, Ca, Mg)_3(Al, Si)_6O_{12}$ (Irifune and Ringwood 1993; Kesson et al. 1994; Ono et al. 2001; Hirose and Fei 2002). Al concentration in the CF phase varies from 32.8 to 45.1 wt% Al_2O_3 (av.: 39.4 ± 3.6 wt% Al_2O_3), independently of Si and pressure values. Representative compositions of the CF phase from experimental data are presented in Table 5.5.

The CF phase has an orthorhombic space group *Pbnm* and four formula units ($Z = 4$ on a four oxygen primitive basis) in the unit cell (Decker and Kasper 1957). Such CF structure is a common high-pressure structure type (Wicks and Duffy 2016) experimentally adopted by several compositions including $MgAl_2O_4$ (Irifune et al. 1991), $CaAl_2O_4$ (Reid and Ringwood 1969), and $NaAlSiO_4$ (Liu 1977). It is one of a series of similar structures ($CaFe_2O_4$, $CaTi_2O_4$, $CaMn_2O_4$) that are common high-pressure polymorphs of spinel-structured phases (Yamanaka et al. 2008). Single-crystal diffraction experiments have shown that forsterite, Mg_2SiO_4, metastably adopts a related structure upon room temperature compression above 58 GPa (Finkelstein et al. 2014). CF structure was established for $FeCr_2O_4$ composition in meteorites (Chen et al. 2003) and suggested a new $CaCr_2O_4$ oxide found in ultramafic lower-mantle microxenolite (Kaminsky et al. 2015; see Sect. 4.7.3).

The CF phase has a chain framework structure formed by edge-sharing AlO_6 octahedra along the *c*-axis direction similar to the NAL phase, but it only forms one kind of 'tunnel' formed by the linked double chains being in eight-fold coordination, where sodium atoms are located (Yamada et al. 1983) (Fig. 5.9). This model is

Table 5.5 Representative compositions of the CF phase from experimental mafic associations (wt%)

Starting material	Powdered MORB composition			Fresh natural MORB		Synthetic MORB glass	
P (Gpa)	30	33	37	44	55	80	100
T (K)				2391	2550		
Sample No.				MORB#4	MORB#5		
Mineral association	Brd + CaSiPrv + Sti + CF			Brd + CaSiPrv + Sti + NAL + CF	Brd + CaSiPrv + Sti + CF		
SiO_2	27.5	27.9	28.9	28.5	26.7	26.0	32.4
TiO_2	0.7	0.7	0.7	0.5	0.2		
Al_2O_3	40.1	37.6	36.6	39.8	43.2	45.1	44.1
FeO	7.9	7.1	6.7	9.7	6.2	9.0	5.9
MgO	10.0	10.0	7.1	11.0	12.9	8.9	7.7
CaO	0.8	1.3	0.5	1.3	1.7	0.8	0.7
Na_2O	12.1	13.2	15.2	9.2	9.1	10.3	9.3
K_2O	0.0	0.0	0.0	n.a.	n.a.	n.a.	n.a.
Total	99.1	97.8	95.7	100.0	100.0	100.1	100.1
fe	0.307	0.285	0.346	0.331	0.212	0.362	0.300
mg	0.693	0.715	0.654	0.669	0.788	0.638	0.700
Al/Si (at.)	1.719	1.589	1.493	1.646	1.907	2.045	1.604
Reference	Ono et al. (2001)			Ricolleau et al. (2010)		Kesson et al. (1994)	

Note n.a. not analysed

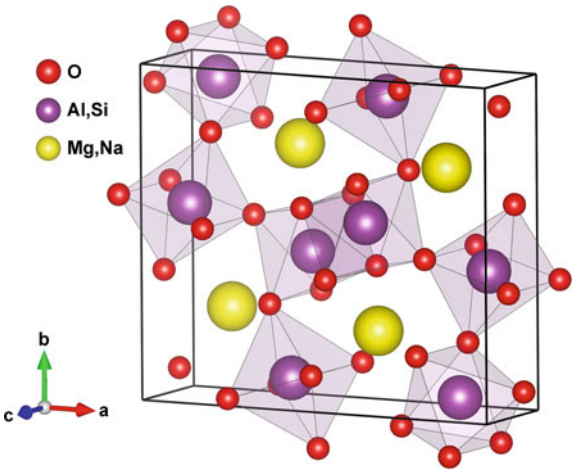

Fig. 5.9 Orthorhombic structure of the CF phase (space group *Pbnm*). Lattice parameters from Kojitani et al. (2007)

based on structural parameters for the $MgAl_2O_4$ end-member (Kojitani et al. 2007), whereas the CF-type phase in basaltic compositions of the lower mantle can exist within the $NaAlSiO_4$–$MgAl_2O_4$ system.

Experimental studies on the $NaAlSiO_4$–$MgAl_2O_4$ system in a laser-heated DAC coupled with in situ synchrotron XRD measurements demonstrated that the CF phase is the high pressure form of the NAL phase, with a transition pressure between 34 and 43 GPa (Ono et al. 2009; Imada et al. 2011). On the other hand, the CF phase exists in association with the NAL phase at pressures of up to 50 GPa (Ono et al. 2009; Ricolleau et al. 2010; Imada et al. 2011), and at much higher pressures of up to 120 GPa and 2300 K, in the potassium-rich system. The calcium-bearing CF phase is also found to coexist with the NAL phase (Kato et al. 2013). Thus far, these studies have shown that the relative stability of NAL and CF phases is a complex, sensitive function of *P*–*T* and composition. While pressure tends to favour stability of the CF phase, enrichment in Mg or alkalis tends to favour the NAL phase (Mookherjee et al. 2012).

The NAL to CF phase transition causes an increase in density and bulk modulus (Guignot and Andrault 2004) and a change in compressional wave velocity by −0.2% and shear wave velocity by +0.9% (Kawai and Tsuchiya 2012); the shear wave velocity increases by 2.5% across phase transition at ∼40 GPa (Dai et al. 2013). The change in the elastic properties and shear wave anisotropy across the NAL to CF phase transition is proposed to be significant enough to be seismically detectable (Kawai and Tsuchiya 2012; Dai et al. 2013). A study on the physical properties of the aluminous phases performed by Mookherjee et al. (2012), demonstrated that the sound wave velocities of the NAL phase is significantly lower than the CF phase and other major lower mantle phases. The existence of such a lower-velocity NAL phase in the deeply subducted MORB materials can compensate for the faster sound velocity of silica (SiO_2) and its high-pressure polymorphic phase(s) in the lower mantle.

5.3.4 Calcium Aluminium Silicate with Ba-Ferrite Structure (CAS Phase)

A Ca–Al silicate (CAS) with an end-member chemical formula of $CaAl_4Si_2O_{11}$ containing some amount of water was first reported by Irifune et al. (1994) in experiments performed at 17.5–24 GPa and 1500–1900 °C, and later by Gautron et al. (1996) at 14 GPa and 1400–1500 °C. The CAS phase has a hexagonal unit cell with lattice parameters a = 5.4 Å and c = 12.7 Å and a space group, most likely, $P6_3/mmc$ with Z = 2, analogous to hexagonal Ba-ferrite $BaTi_2Fe_4O_{11}$. It has a six-layer, close-packed structure, reasonable for a phase stable under the conditions of the transition zone (Gautron et al. 1997).

Subsequently, the CAS phase was synthesized as an Al-rich phase using anhydrous MORB materials in multi-anvil apparatus at 25.5 GPa (Hirose and Fei 2002; Litasov and Ohtani 2005). In these experiments, the NAL and CF phases appeared at higher pressures, above 27–27.5 GPa, coexisting with bridgmanite, stishovite and CaSi-perovskite. The NAL phase synthesized at 26 GPa was stable below 2030 °C but transformed to the CAS phase at higher temperatures. The CAS phase does not appear below the solidus temperature in the presence of bridgmanite. It remains unclear whether the CAS phase can present in the lower mantle.

In the natural environment, a single sample of CAS in association with kyanite was reported from an inclusion in Juina-5 kimberlite pipe, Brazil (Thomson et al. 2014). The natural CAS is poorer in Mg and Al (with Al/Si = 1.027) than when obtained from experiments (Table 5.6).

5.4 Partitioning of Aluminium Between Bridgmanite and Aluminous Phases

Aluminium in the lower-mantle mafic association has been observed to be concentrated in three major phases: bridgmanite, NAL phas, and CF phase. The concentration of Al in bridgmanite of the mafic association varies from 11 to 13 wt% Al_2O_3 at 26 GPa to 24 wt% Al_2O_3 at 100 GPa (see Fig. 5.1), independently of the magnesium index value (mg), which is rather constant. Al-rich NAL phase with 38.9–53.8 wt% Al_2O_3 (average: 46.2 ± 4.9 wt% Al_2O_3) probably incorporated its aluminium from majorite in the lower mantle, and shows a strong correlation of its Al_2O_3 concentration with SiO_2 (Fig. 5.7a). The ratio Al/Si_{at} in the NAL phase strongly decreases from 4.7 at 25 GPa to 1.73 at 33 GPa (Fig. 5.7b). Al concentration in the CF phase varies from 32.8 to 45.1 wt% Al_2O_3 (average 39.4 ± 3.6 wt % Al_2O_3), independently of Si and pressure values. This implies that with redistribution of Al between bridgmanite and NAL occurs with increasing pressure, as subducting slabs penetrate deeper into the lower mantle.

Table 5.7 shows Si/Al ratio values in coexisting bridgmanite in the NAL phase from the experimental solidus associations, as well as Al/Si ratios and aluminium partitioning coefficient values. The partition coefficient of aluminium between bridgmanite and the

Table 5.6 Compositions of synthetic and natural CAS phase (wt%)

Starting material	Glass with a natural MORB composition	Synthetic MORB glass	Juina-5 pipe, Brazil
P (Gpa)	27.5	26.5	n/a
T (K)	2703	2523	n/a
Sample No.	LO#117	K-255	Ju5-85
Mineral association	Brd + CaSiPrv + Sti + NAL + CAS + Liq	Brd + CaSiPrv + Sti + NAL + CAS + Liq	CAS + Ky
SiO_2	41.99	37.50	40.19
TiO_2	0.26	0.46	0.79
Al_2O_3	39.65	44.40	35.03
Cr_2O_3	0.07	n.a.	0.07
FeO	1.80	1.43	1.50
NiO	n.a.	n.a.	0.05
MnO	0.03	n.a.	0.02
MgO	2.92	1.76	0.31
CaO	11.08	12.70	16.88
Na_2O	1.28	1.17	3.59
K_2O	1.07	0.32	0.80
Total	100.15	99.74	99.23
fe	0.257	0.313	0.731
mg	0.743	0.687	0.269
Al/Si (at.)	1.113	1.396	1.027
Reference	Hirose and Fei (2002)	Litasov and Ohtani (2005)	Thomson et al. (2014)

Note n.a. not analysed

Table 5.7 Si/Al ratio values (atomic) and partition coefficient of Al in coexisting bridgmanite and NAL

Sample No.	Mineral association*	Pressure, GPa	Al/Si in bridgmanite	Al/Si in NAL	$K_D^{Brd–NAL}$	Reference
K-156	Brd + CaSiPrv + Sti + NAL	25	0.463	4.698	0.099	Litasov and Ohtani (2005)
K-206wet	Brd + CaSiPrv + Sti + NAL	26	0.472	4.094	0.115	Litasov and Ohtani (2005)
mbk-1	Brd + CaSiPrv + Sti + NAL + CF + Maj	26.1	0.321	2.408	0.134	Litasov et al. (2004)
K-244wet	Brd + CaSiPrv + Sti + NAL	28	0.512	3.781	0.136	Litasov and Ohtani (2005)
K-244dry	Brd + CaSiPrv + Sti + NAL	28	0.409	2.760	0.148	Litasov and Ohtani (2005)
K-254	Brd + CaSiPrv + Sti + NAL	28	0.555	2.326	0.238	Litasov and Ohtani (2005)
–	Brd + CaSiPrv + Sti + NAL + CF	33	0.348	1.730	0.201	Ricolleau et al. (2010)
–	Brd + CaSiPrv + Sti + NAL + CF	44	0.591	2.277	0.260	Ricolleau et al. (2010)

Note *The associations with liquid are not included

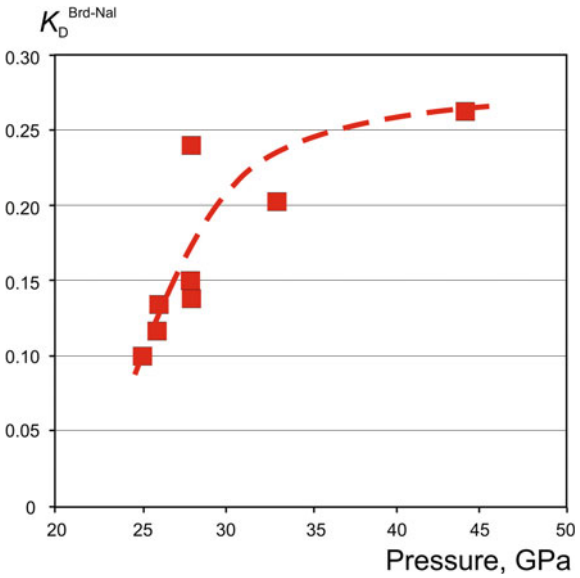

Fig. 5.10 Dependence of aluminium partition coefficient $K_D^{Brd–NAL}$ of pressure

NAL phase defined as $K_D^{Brd–NAL} = (Al/Si)^{Brd}/(Al/Si)_{at}^{NAL}$ varies from 0.10 to 0.26, asymptotically increasing within a pressure range of 25–44 GPa (Fig. 5.10). This confirms that the Al enrichment in bridgmanite with increasing pressure is a result of the dissolution of the NAL phase, while the Al concentration in the CF phase, which replaces the NAL phases at pressures of 40–50 GPa, remains constant. The Al concentration in bridgmanite, after reaching a maximal concentration of ~24–25 wt%, also remains constant.

5.5 Hydrous Aluminous Phases

5.5.1 General

Subducting slabs can contain significant amounts of water in hydrous minerals in hydrothermally altered basalts (e.g., serpentine) and sediments (e.g., clay minerals). High-pressure investigations of the Al_2O_3–SiO_2–H_2O system relevant to subducting slab materials have found that three hydrous mineral phases, phase Egg, δ-AlOOH and topaz-OH can possibly become stable at *P–T* conditions corresponding to the lower mantle. Initially, however, these three phases were reported to be stable at relatively lower *P–T* conditions at 5.5–21 GPa and temperatures up to 1500 °C (Wunder et al. 1993; Schmidt 1995; Ono 1999; Suzuki et al. 2000). Subsequently, they were experimentally proven to be stable at greater depths relevant to the lower-mantle conditions. Phase Egg and δ-AlOOH are found as inclusions in natural diamonds.

5.5.2 *Phase Egg*

A hydrous aluminous silicate $AlSiO_3OH$ was first observed in high-pressure experiments on hydrous basaltic systems at pressures exceeding 10 GPa. The first water-containing high-pressure mineral, initially suggested as $Al_5Si_5O_{17}OH$ (Egglton et al. 1978):

$$AlOOH + SiO_2 \rightarrow AlSiO_3OH.$$
$$\text{diaspore} + \text{stishovite} \rightarrow \text{phase Egg}$$

This phase was subsequently synthesized from topaz-OH + stishovite mixture at 12 GPa, and has been later termed as phase Egg to give credit to Professor R.A. Egglton who first discovered the phase (Egglton et al. 1978; Schmidt 1995). High *P–T* stability of the phase was experimentally extended to 20 GPa and 1700 °C (Ono 1999), then to 23 GPa and 1200 °C (Sano et al. 2004), then to 25 GPa and ~1500 °C (Boffa Ballaran et al. 2010), and later to 26 GPa and 1460 °C (Pamato et al. 2015). Most recently Fukuyama et al. (2017) experimentally established the stability limit of phase Egg at 23.5 GPa, suggesting that differences in previous results were caused by the use of different pressure scales. They concluded that phase Egg is stable only within the transition zone (Fukuyama et al. 2017). However, other experiments and equation of state study of this phase demonstrate that, despite the presence of hydrogen in its composition, phase Egg is stable up to 40 GPa (Vanpeteghem et al. 2003). For this reason, the presence of phase Egg and stishovite in natural samples may be suggestive not only of the origin in the transition zone but in the lower mantle as well, and phase Egg may be considered as a major carrier of water in the deep Earth.

A natural association of stishovite and phase Egg was observed in a diamond from the Rio Soriso, Juina area, Brazil (Wirth et al. 2007) (Fig. 5.11). Both minerals were identified with the observation of in situ Raman spectroscopy and electron diffractometry, such that original mineral structures were not altered during the examination.

Phase Egg forms an aggregate of euhedral, cubic and cubo-octahedral grains that are 20–30 to 200–300 nm in size (Fig. 5.11b). The bulk Si/Al ratios of the two analyzed natural grains are approximately 1:1 (46.74–53.84 at.% and 45.63–52.60 at.%). A minor admixture of Fe (0.29–1.52 at.%) is present in its composition. The presence of OH in phase Egg was identified using the pre-peak at approximately 528 eV in the electron energy-loss spectrum and the OH-stretching band between 1800 and 3000 cm^{-1} in the Raman spectra. Numerous irregularly shaped pores are present in the stishovite matrix (Fig. 5.11a). They contained a fluid, which was released to the vacuum during the focused ion beam milling of the specimen for the transmission electron microscopy analysis. Quench products of the fluid contain minor amounts of K, Ca, Ba, P, S, Cl and F that were also detected along the walls of the pores. This porosity possibly reflects the initial stage of degassing of phase Egg under conditions close to its pressure-dependent disintegration. In some of the Raman spectra taken from phase Egg, characteristic spectral features of δ-AlOOH

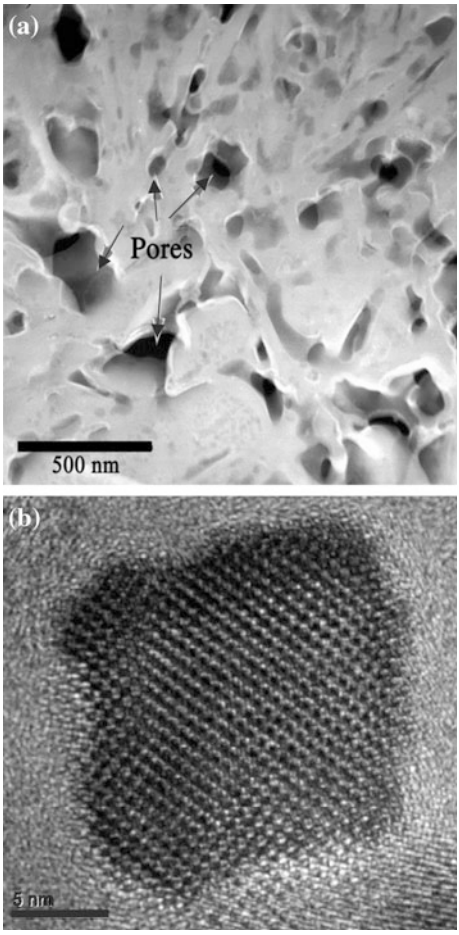

Fig. 5.11 Electron-microscope images of phase Egg. **a** Porous aggregate of stishovite and phase Egg. **b** Single cubic crystal of phase Egg. From Wirth et al. 2007. © Earth and Planetary Science Letters (Elsevier)

phase located near 2150 and 2500 cm^{-1} were detected, analogous to the spectral characteristics of experimentally produced δ-AlOOH phase (Ohtani et al. 2001b). The coexistence of δ-AlOOH phase with phase Egg indicates the most likely pressure interval for their joint formation to be 23–27 GPa, i.e., in the uppermost regions of the lower mantle (Sano et al. 2004).

The crystal structure of phase Egg, obtained in experimental studies, was determined, using powder XRD, to be monoclinic (Fig. 5.12) with a space group $P2_1/n$, a unit cell volume $V_0 = 212.99(1)$ $Å^3$, and zero-pressure density of 3.74 g/cm^3 (Schmidt et al. 1998). Most grains of natural phase Egg are monoclinic as well, but

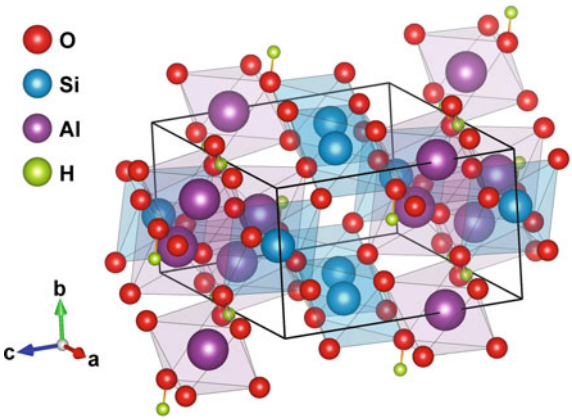

Fig. 5.12 Monoclinic crystal structure of phase Egg (space group $P2_1/n$) with lattice parameters from Schmidt et al. (1998)

some analyzed natural grains are tetragonal (a = 0.7435 nm and c = 0.706 nm), suggesting that the tetragonal polymorph may be a relic of the original phase Egg.

The monoclinic structure of phase Egg resembles that of stishovite and δ-AlOOH, containing an ordered arrangement of SiO_6 and AlO_6 octahedra linked by both edge- and corner-sharing (Fig. 5.12). Similar to δ-AlOOH (see Sect. 5.5.3), the crystal structure of phase Egg is characterized by strong hydrogen bonding, which can have great effects on many of the properties in the mineral including elasticity, rheology and electrical conductivity. Hydrogen bonding, which is the electrostatic attraction between two polar groups (in this case hydrogen and oxygen atoms), also plays an important role in stabilizing hydrous and nominally anhydrous phases by lowering the enthalpy, or increasing the entropy, or both (e.g., Prewitt and Parise 2000). The strong hydrogen bonding in phase Egg and δ-AlOOH (as well as in DHMSs) may be an important factor in stabilizing these structures at high pressures and temperatures.

5.5.3 *Hydrous δ-AlOOH and ε-FeOOH Phases*

Aluminium oxyhydroxide, the hydrous δ-AlOOH phase, which is a high-pressure polymorph of diaspore (α-AlOOH) and boehmite (γ-AlOOH), was initially synthesized in association with majorite and phase Egg at ~21 GPa and 1000 °C (Suzuki et al. 2000). Subsequently, it has been found to be stable at pressures above 30 GPa and temperatures of 1000–1200 °C, and thus it may serve (like phase Egg) as a water carrier in the cold subducted slabs, transporting water into the lower mantle (Ohtani et al. 2001a, b; Sano et al. 2004). Later, in situ XRD experiments in the diamond anvil cell were conducted to determine the stability field of δ-AlOOH over the entire P–T conditions of the lower mantle. δ-AlOOH was observed to exist at pressures from 33 to 134 GPa at 1350–2300 K, indicating that this hydrous mineral in the sediment layer of a subducting slab could transport water into the

core-mantle boundary (Sano et al. 2008; Mashino et al. 2016). The experiments by Ohira et al. (2014) also confirmed that a hydrous δ–AlOOH phase could coexist with Al-depleted bridgmanite or post-perovskite under the *P–T* conditions relevant to the cold slab geotherm. δ-AlOOH was identified in geological samples to exist in association with phase Egg (Wirth et al. 2007).

Theoretical calculations further predicted the pressure-induced phase transition of δ-AlOOH into a new cubic phase at approximately 170 GPa (Tsuchiya and Tsuchiya 2011). Therefore, δ-AlOOH phase is likely to be the highest pressure phase among all hydrous mineral compounds, since these hydrous materials tend to dissociate and release H_2O at pressures of around a few tens of GPa (Ohtani et al. 2001b).

Pure δ-AlOOH has an orthorhombic symmetry with a non-centrosymmetric space group $P2_1nm$ that is very close to that of SiO_2 in the $CaCl_2$-type (Suzuki et al. 2000; Komatsu et al. 2006; Vanpeteghem et al. 2007) (Fig. 5.13a). The structure contains both AlO_6 and HO_6 octahedra, and the oxygen anions form a slightly distorted hexagonal close-packed arrangement perpendicular to the *b* direction

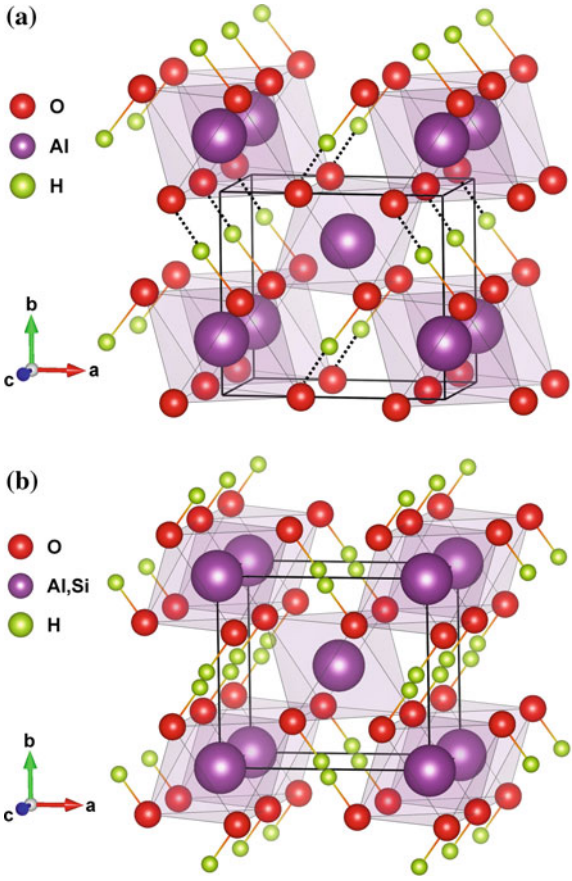

Fig. 5.13 Orthorhombic crystal structure models of δ-AlOOH based on $P2_1nm$ and *Pnnm* space groups. *Dotted lines* are partially ordered H bonds. Unit cell parameters from Komatsu et al. (2011)

(Wicks and Duffy 2016). A single-crystal XRD study indicates that δ-AlOOH transforms to the $CaCl_2$-type structure (space group *Pnnm*) at ~8 GPa (Kuribayashi et al. 2013) (Fig. 5.13). This structure consists of corner-sharing chains of edge-sharing octahedra (AlO_6, in this case). There is no discontinuity in unit cell volume across this displaceable transition. The main difference between the two structures lies in the disordering of hydrogen atoms in the high-pressure structure. The substitution of Mg^{2+} and Si^{4+} into δ-AlOOH also promotes the transformation of $P2_1nm$ structure (Suzuki et al. 2000; Kudoh et al. 2004; Komatsu et al. 2011). The disordered cations, Mg^{2+} and Si^{4+}, with different valences than Al^{3+} may fluctuate hydrogen positions, causing the disordered hydrogen to change its symmetry. As a result, Mg–Si-containing δ-AlOOH phase exhibits the *Pnnm* structure (Komatsu et al. 2011) or *Pnn*2 structure (Kudoh et al. 2004).

Pressure-induced hydrogen bond symmetrization starts to occur in δ-AlOOH at 28 GPa (Tsuchiya et al. 2002), similar to that reported for phase Egg. Since the crystal structure with the symmetric hydrogen bonding has a smaller volume than the asymmetric hydrogen bond counterpart, the occurrence of the hydrogen bond symmetrisation can further stabilize hydrous materials to higher-pressure conditions. It is conceivable that higher-pressure hydrous phases would also be expected to have symmetric hydrogen bonds. The details of the hydrogen bonding in δ-AlOOH phases has been extensively discussed, especially with regards to the formation of symmetric hydrogen bonds, but there is currently no consensus on this issue (Tsuchiya et al. 2002; Panero and Stixrude 2004; Li et al. 2006; Xue et al. 2006; Vanpeteghem et al. 2007; Sano-Furukawa et al. 2008).

The predicted ultrahigh-pressure cubic phase has a cubic pyrite-type AlO_2 framework with interstitial H atoms forming symmetric hydrogen bonds, whose symmetry is assigned to the space group $Pa\bar{3}$.

Other cation substitutions, such as Fe and Ti in the oxyhydroxide, have also been suggested based on high *P*–*T* experiments corresponding to the transition zone conditions: at pressures of 16 GPa and temperatures of 1000–1600 °C (Nishihara and Matsukage 2016). In the studied conditions, two stable iron-titanium oxyhydroxide phases were identified whose estimated composition is $(FeH)_{1-x}Ti_xO_2$. One is the Fe-rich solid solution ($x < 0.23$) with ε-FeOOH-type crystal structure (orthorhombic, *P*21 *nm*); and the other is the more Ti-rich solid solution ($x > 0.35$) with α-PbO_2-type structure (orthorhombic, *Pbcn*). The ε-FeOOH-type phase is stable up to ~1100 °C, whereas the Ti-rich α-PbO_2-type phase is stable up to 1500 °C for a composition of $x = 0.5$ and at least to 1600 °C for $x = 0.75$. These phases may be stable within subducting basaltic slabs into the transition zone, but their stability in the lower mantle remains uncertain and requires further clarifications in future studies.

In iron-rich compositions, a complete Fe–Al substitution may occur. ε-FeOOH, the high-pressure polymorph of goetite (α-FeOOH), is isostructural with δ-AlOOH, and has a slightly distorted rutile structure with corner-linked single bands of edge-shared octahedra parallel to the *c*-axis (Otte et al. 2009). ε-FeOOH undergoes a spin transition beginning at 49 GPa and completing at ~65 GPa, which is

assisted by symmetrization of hydrogen bonds during the transition from $P2_1nm$ to *Pnnm*. (Gleason et al. 2008, 2013; Reagan et al. 2016).

5.5.4 Topaz-OH

Topaz-OH $Al_2SiO_4(OH)_2$, the OH end-member of the F-OH topaz, has been synthesized at a pressure of 6–10 GPa from diaspore (α-AlOOH) and phase Π $Al_3Si_2O_7(OH)_3$ starting materials as a result of their reaction with SiO_2. This phase is shown to be stable up to 13 GPa and 1500 °C (Wunder et al. 1993; Xue et al. 2006), after which it reacts with SiO_2 to form phase Egg $AlSiO_3OH$ (Egglton et al. 1978; Schmidt 1995, 1998; Ono 1999). At high temperatures, it undergoes a dehydration reaction to form kyanite (Wunder et al. 1993). At pressures above 14 GPa, a high-pressure topaz-OH II variety, with significant cation disorder occurs (Kanzaki 2010).

The structure of topaz-OH shows close agreement with that of F-rich topaz, containing tetrahedral SiO_4 and linked $AlO_4(OH)_2$ octahedra. It was first refined with the space group *Pbnm* from single-crystal XRD by Wunder et al. (1993), although the hydrogen positions could not be located. A subsequent single-crystal XRD study (Northrup et al. 1994) reported that the single H position found in F-rich topaz is split into two nonequivalent, half-occupied H positions in topaz-OH. They also suggested that the structure is non-centrosymmetric and might have a long-range ordered H distribution with a reduction of symmetry to $Pbn2_1$. Each H is associated with three O atoms in an irregular trifurcated H-bond arrangement. A lattice energy calculation and molecular dynamics simulation study (Churakov and Wunder 2004) predicted four nonequivalent crystallographic H positions in topaz-OH that are in dynamic exchange at ambient conditions and suggested instantaneous configuration of H violates in all symmetry elements, whereas the space- and time-averaged structure possesses *Pbnm* symmetry. Monoclinic structure $P2_1/c$ is also suggested for topaz-OH (Mookherjee et al. 2016).

The stability of topaz-OH under high *P–T* conditions has not been studied.

5.6 Dense Hydrous Magnesium Silicates (DHMSs)

5.6.1 General

Numerous experimental high-pressure works were carried out on DHMSs of relevant mantle compositions, showing that they can be stable with increasing pressure at characteristic slab temperatures. Ringwood and Major (1967) recognized the first of these DHMSs in experiments performed in the MgO–SiO–H_2O system under pressures of up to 18 GPa, and denoted these phases as A [$Mg_7Si_2O_8(OH)_6$], B [$Mg_{12}Si_4O_{19}(OH)_6$], and C, known also as superhydrous Phase B

$[Mg_{10}Si_3O_{14}(OH)_4]$. The naming system for the DHMS phases proposed by them was later adopted for naming a whole sequence of 'alphabetic' DHMS phases. Phases termed D (Yamamoto and Akimoto 1977; Liu 1986, 1987), E, F (Kanzaki 1989, 1991; Kudoh et al. 1993, 1995), and G (Ohtani et al. 1997) were subsequently reported; however the latter two, F and G, appear to be similar if not identical to Phase D (Yang et al. 1997; Frost and Fei 1998, 1999). These phases contain 2.14–18 wt% H_2O and may act as water carriers in subducting hydrated plates to >35 GPa (Yang et al. 1997; Ohtani et al. 2004), in addition to hydrous aluminium phases. Most of these phases appeared to be unstable under lower-mantle pressure conditions (e.g., Kanzaki 1991), with the exception of the following three: superhydrous Phase B, Phase D, and the recently discovered Phase H.

5.6.2 *Superhydrous Phase B*

'Superhydrous' Phase B $[Mg_{12}Si_4O_{19}(OH)_6]$, containing as much as 5.8 wt% H_2O, is stable at *P–T* conditions relevant to the top of the lower mantle and decomposes into periclase, bridgmanite and Phase D at approximately 30 GPa and high temperatures (Shieh et al. 1998). On the other hand, the following reaction sequences were observed with increasing temperature from 1200 to 1600 °C in the pressure range from 18–20 GPa: superhydrous Phase B → Phase B + liquid → wadsleyite + periclase + liquid → anhydrous Phase B + periclase + liquid (Ohtani et al. 2001a).

5.6.3 *Phase D*

Initially, the term Phase D was used by Yamamoto and Akimoto (1977) to describe the hydroxyl chondrodite, which was synthesized at pressures between 3 and 12 GPa. However, Liu (1987) reapplied the name Phase D to describe a phase discovered as a dissociation product of $Mg_3Si_2O_5(OH)_4$ serpentine at pressures above ~20 GPa (an equivalent to phases F and G). It has the ideal formula $MgSi_2O_6H_2$ (Mg-Phase D), but is typically non-stoichiometric. Phase D contains nominally 10.1 wt% H_2O (varying from 10 to 18 wt%) and varies significantly in stoichiometry depending on synthesis conditions (Frost and Fei 1998) with Mg/Fe ratio from 0.56 to 0.71 within the range of 16–27 GPa and 1073–1573 K; the Mg/Si ratio and H_2O concentration decrease with increasing temperature and increase with increasing pressure (Shinmei et al. 2008). Along with most other DHMS phases, Phase D synthesized from the starting samples containing complex peridotitic bulk compositions have been found to contain up to 7 wt% Al_2O_3 and 5 wt% FeO (Frost 1999; Litasov et al. 2007b, 2008; Rosa et al. 2012; Ganskow and Langenhorst 2014), suggesting that natural Phase D samples contain not only water but also some Al and Fe. Al^{3+} substitutes for Si^{4+}, Fe^{2+} substitutes for Mg, and Fe^{3+} may occupy Si and Mg sites (Ganskow and Langenhorst

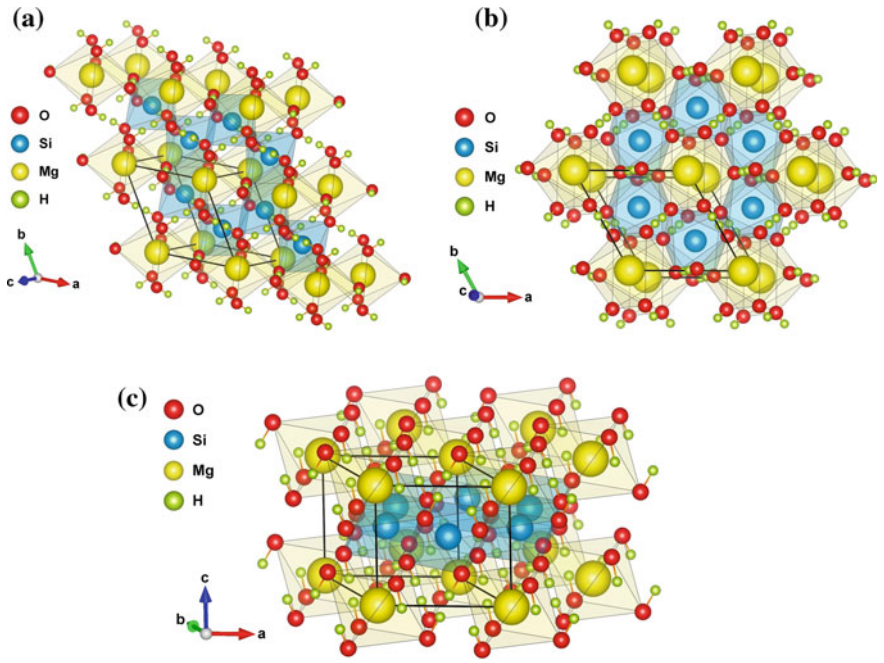

Fig. 5.14 Crystal structure of Al-free trigonal phase D (space group *P*-31*m*) in different axis orientations. Lattice parameters from Yang et al. (1997)

2014). Available data demonstrate that the $Fe^{3+}/\Sigma Fe$ ratio of Fe-bearing phase D determined by conventional Mössbauer spectroscopy and EEL spectroscopy is 0.60–0.94, and iron is not involved in water-substitution mechanisms (Chang et al. 2013; Ganskow and Langenhorst 2014).

Phase D has a trigonal structure with the space group *P*-31 *m*, based on a hexagonal close-packed array of oxygen atoms (Kudoh et al. 1997; Yang et al. 1997; Xue et al. 2008), similar to stishovite (Fig. 5.14). All cations except H are in the octahedrally coordinated sites. The MgO_6 and SiO_6 octahedra occur in separated, alternating layers stacked along the *c* direction (Fig. 5.14c), with Mg and Si at the M1 and M2 sites, respectively, and with the octahedral sites corresponding to the 2*c* (M3) and 1*b* Wyckoff positions being vacant (Yang et al. 1997). The MgO_6 and SiO_6 octahedra share edges with neighbours to form rings in layers perpendicular to the *c* axis (Fig. 5.14b). The SiO_6 octahedra form gibbsite-like layers, in which each octahedron shares three edges, leaving one third of the octahedral sites vacant. The MgO_6 octahedra lie above and below vacant sites in the SiO_6 layer and are corner-linked to the Si octahedra, and so two thirds of the Mg octahedral sites are empty (Wicks and Duffy 2016). Charge balance is achieved by hydrogen anions. The hydrogen positions are located in the MgO_6 layers, with O–H bonds facing away from SiO_6 octahedra.

Phase D is the only DHMS structure reported to date that contains Si exclusively in octahedral co-ordination. Owing to this, the calculated density of Phase D is 3.50 g/cm^3, which is substantially greater than any other DHMS found thus far, including Phase A (2.96 g/cm^3), Phase B (3.37 g/cm^3), superhydrous Phase B (3.21 g/cm^3), Phase E (2.82 g/cm^3), and Phase F (Yang et al. 1997 and references therein). As a result of the layered nature of the structure, with strong SiO_6 layers alternating with weaker MgO_6 octahedra resulting in enhanced compressibility along the *c* axis, Phase D exhibits anisotropic compression (Frost and Fei 1999). Theoretical calculations of the elastic constants indicate that the anisotropy decreases with depth but significant anisotropy in seismic wave velocities is retained to the highest pressures (Mainprice et al. 2007).

At pressures exceeding 35–40 GPa Phase D, like phase Egg and δ-AlOOH (see above), experiences hydrogen bond symmetrization (Tsuchiya et al. 2005; Shinmei et al. 2008). A symmetric hydrogen bond is one in which the hydrogen atom is located at the midpoint between the two neighbouring oxygen atoms, rather than the asymmetric O–H distances that characterize a conventional hydrogen bond. This serves stabilizing hydrous Phase D (as well as phase Egg and δ-AlOOH) under ultrahigh-pressure conditions. This pressure-induced hydrogen bond symmetrization has a significant effect on the compression behaviour of Phase D. The bulk modulus increases by about 20% with this structural change (Tsuchiya et al. 2005). A powder XRD study showed evidence of such an anomaly (Hushur et al. 2011), but a more recent high-resolution single-crystal XRD study to 65 GPa found no evidence for a bulk modulus anomaly, at least to this pressure (Rosa et al. 2013a, b). No evidence for hydrogen bond symmetrization was found in an infrared spectroscopic study (Shieh et al. 2009) or in other theoretical calculations (Mainprice et al. 2007).

Fe-bearing Phase D was reported to undergo the electron spin transition of Fe^{3+} at high pressure, which is shown to cause a softening in the bulk modulus and bulk sound velocity of the crystal (Chang et al. 2013). Recently, a two-stage HS-LS spin transition involving both Fe^{2+} and Fe^{3+} was reported to occur in Phase D at high pressures (Wu et al. 2016b). This transition of iron occurs for Fe^{2+} at 37–41 GPa and for Fe^{3+} at 64–68 GPa. These transitions are accompanied by an increase in density and a significant softening in the bulk modulus and bulk velocity at their respective pressure range. The occurrence of the dense low-spin FeAl-bearing phase D with relatively high velocity anisotropies in deep-subducted slabs can potentially contribute to small-scale seismic heterogeneities. However, hydrogen symmetrization and spin transitions in Phase D may overlap with each other, and their interplay at high pressures is not yet fully understood (Wu et al. 2016b).

The stability field of Phase D extends from 20 to 50 GPa, independent of temperature from ~1300–1700 K (Shieh et al. 1998, 2000; Frost and Fei 1998, 1999; Tsuchiya et al. 2005; Litasov et al. 2008; Shinmei et al. 2008; Hushur et al. 2011; Ghosh and Schmidt 2014; Nishi et al. 2014; Walter et al. 2015). Pure Phase D is stable only at relatively lower temperatures and can break down at temperatures lower than those of the typical mantle geotherm (e.g., Nishi et al. 2014). In experiments, Phase D decomposes at 44–50 GPa, corresponding to a

depth of 1250–1400 km, into an assemblage of nominally anhydrous phases consisting of low-Al bridgmanite and H_2O (Shieh et al. 1998; Walter et al. 2015).

The more stable, Al-rich variety of Phase D with up to 50 wt% Al_2O_3 was synthesized in association with phase Egg in a simplified basaltic bulk composition at lower mantle conditions at 25 GPa and ~1500 °C, which is significantly higher than temperature stability for pure Phase D, allowing the Al-rich Phase D to remain stable and host H_2O in the subducting oceanic crust in the Earth's lower mantle (Boffa Ballaran et al. 2010). This idea was confirmed by experiments that demonstrated that Al-rich Phase D $Al_2SiO_6H_2$ in association with phase Egg and stishovite, has very high thermal stability extending to over 2000 °C at 26 GPa, i.e., higher than the expected geotherm of the normal lower mantle (Pamato et al. 2015). In the subsolidus, the Al-rich Phase D is stable to ~55 GPa (Walter et al. 2015). The Al-rich Phase D may have an admixture of Fe, which actually decreases its stability (Ghosh and Schmidt 2014). According to experimental data, Al/Fe ratios in Phase D and in coexisting bridgmanite are roughly equal (Pamato et al. 2015).

The Al-rich Phase D was suggested initially to have the same structure as Mg-Phase D (space group *P*-31*m*), but with a more disordered cation distribution (Boffa Ballaran et al. 2010). A more recent study by Pamato et al. (2015) attributes its structure to hexagonal with the space group $P6_3/mcm$, where Al replaces Mg and all six octahedral sites become partially occupied by a random and disordered distribution of Si and Al, such that M1 and M4 become equivalent (as do M2 and M3), resulting in an increase in symmetry. One of the main differences between the structures is that the Al–Si disorder in Al-rich Phase D results in essentially an undistorted octahedra of similar size, whereas in Mg-Phase D, large MgO distances cause the octahedra to be strongly distorted. The lesser extent of the octahedral distortion is likely to stabilize the Al-rich Phase D relative to its Mg-bearing counterpart. On the other hand, Bindi et al. (2015) reported no change in the unit-cell volume in Al-rich Phase D with respect to pure $MgSi_2O_6H_2$. Earlier, Boffa Ballaran et al. (2010) and Komatsu et al. (2011) observed that the Tscher-mak's $Si^{4+} + Mg^{2+} \rightarrow 2Al^{3+}$ substitution, in hydrous silicates, does not induce either an enlargement of the unit cell or a lengthening of the octahedral bond distances.

An important factor in the charge distribution in the Al-rich Phase D is the large degree of Al–Si disorder. Although the contribution to the configurational entropy due to Al–Si disorder has a stabilizing influence on low-pressure minerals, such as feldspar, the preference of Al for the octahedral site over the tetrahedral coordination at pressures of a few gigapascals means that this effect plays only a minor role in much of the upper mantle and transition zone, such disorder seems to become important again in the lower mantle, where Si and Al both exist exclusively in the octahedral coordination. The Al-rich Phase D may be the first member of a new class of completely disordered hydrous aluminosilicates that consequently have high thermal stabilities (Pamato et al. 2015) (Fig. 5.15).

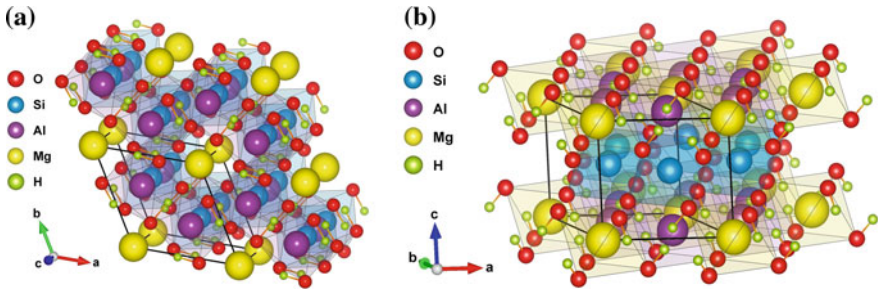

Fig. 5.15 Crystal structure of the Al-rich hexagonal phase D (space group $P6_3/mcm$) in different axis orientations. Lattice parameters from Pamato et al. (2015)

5.6.4 *Phase H*

Using theoretical calculations, Tsuchiya (2013) predicted that Phase D should undergo a phase transition to a new hydrous (with ~15% of water) Phase H with an ideal formula of $MgSiO_4H_2$, in association with SiO_2 ($MgSi_2O_6H_2 \rightarrow MgSiO_4H_2 + SiO_2$) at pressures exceeding ~40 GPa. Subsequently, multi-anvil apparatus experiments using sintered diamond anvils and in situ X-ray measurements showed that Phase D transforms to an assemblage containing Phase Hat pressures above 44–50 GPa (Nishi et al. 2014; Ohtani et al. 2014; Walter et al. 2015).

The crystal structure of Phase H was initially suggested as non-centrosymmetric orthorhombic with a space group $P2_1nm$ similar to the one of the high-pressure hydrous phase δ-AlOOH (Suzuki et al. 2000). Later, Tsuchiya (2013) suggested that it should have a monoclinic symmetry with a space group $P2/m$. However, single-crystal XRD study on Phase D synthesized at 45 GPa unequivocally showed the orthorhombic symmetry with the $CaCl_2$-structure (space group $Pnnm$) (Bindi

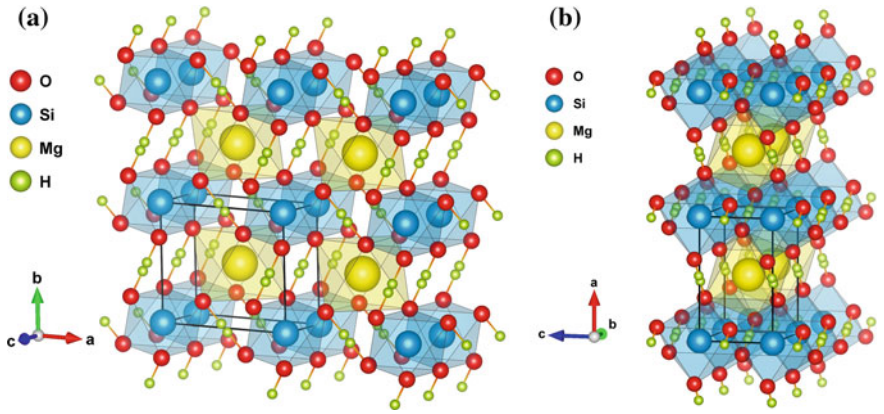

Fig. 5.16 Orthorhombic crystal structure model of phase H (space group $Pnnm$) in different axis orientations. Lattice parameters from Bindi et al. (2014)

et al. 2014). In this structure, Mg^{2+} and Si^{4+} are disordered over the octahedral sites. Distorted Mg and Si octahedra are charge compensated for by H^+ ions, which may occupy one of two positions depicted between the octahedra (Fig. 5.16). When cations with different valence states (i.e., Mg^{2+}, Al^{3+}, and Si^{4+}) become disordered at the octahedral sites, a fluctuation of the hydrogen position occurs to maintain the charge neutrality. Similar to δ-AlOOH, phase Egg and Phase D, the hydrogen bond symmetrization also occurs in Phase H at high pressure, and the hydrogen bond of this phase is already symmetric at the transition from Phase D at 40 GPa (Tsuchiya 2013). Like in Phase D, the hydrogen bond symmetrization probaby helps to stabilize hydrous materials under high-pressure conditions.

Tsuchiya (2013) predicted that pure Phase H had a narrower stability field near 52 GPa at static 0 K, above which it would dissociate into bridgmanite and H_2O (ice VIII). This coincides with experiments performed by Ohtani et al. (2014), in which the stability field of pure Phase H was limited at *P–T* conditions up to 60 GPa and ~1600 K, above which Phase H decomposes into bridgmanite and H_2O.

Considering that Mg- and Si-containing δ-AlOOH has the same as Phase H *Pnnm* structure (Komatsu et al. 2011), one may suggest that Phase H ($MgSiO_4H_2$) and δ-AlOOH ($AlAlO_4H_2$) could form a complete solid solution at high pressures (Bindi et al. 2014). Experiments have shown that intermediate Al-rich compositions can be synthesized together with perovskite and post-perovskite under slab geotherm conditions (Ohira et al. 2014). In association with Phase D, Phase H contains little Al, which strongly partitions into Phase D. At pressure above ~50 GPa, where Phase D is no longer stable, Phase H has the ability to incorporate a significant amount of Al, present in hydrous compositions in the deep lower mantle (Bindi et al. 2015). In this case, the effect of the Al component in Phase H is expected to extend its stability field, which is similar to that in Phase D. Phase H may be considered as an end-member of hydrous-phase solid solution AlOOH–$MgSiO_4H_2$. Experiments by Ohira et al. (2014) in a high-pressure DAC demonstrated that at 68 GPa and 2010 K, hydrous δ-phase contains at least 44 mol% of $MgSiO_4H_2$ component; at 128 GPa and 2190 K, it contains 23 mol% of Phase H component. In other series of the DAC experiments in system MgO–Al_2O_3–SiO_2–H_2O, Phase H was stable between ~45 and 115 GPa in all bulk compositions studied (Walter et al. 2015). Most recent experiments in the $MgSiO_4H_2$–AlOOH–SiO_2 system within the 20-60 GPa pressure range demonstrated that phase H and δ-AlOOH form an ideal mixture and that hydrogen in phase H is bonded in a single well at all pressures, and only the pure phase results in pressure-induced symmetrization, while the solid solution maintains asymmetric bonding to high pressure (Panero and Caracas 2017). Thus, Phase H and δ-AlOOH are likely to be stable hydrous phases in the slabs and transport significant amounts of water into the deep lower mantle.

The presence of hydrogen in the lower mantle may influence other phase transitions. It sharpens the width of the bridgmanite to post-perovskite transition. The unit cell volume of bridgmanite at ambient conditions increases systematically with increasing synthesis pressure above ~55 GPa, possibly representing an increase in Al concentration and potentially hydrogen concentration with depth (Inoue et al. 2010).

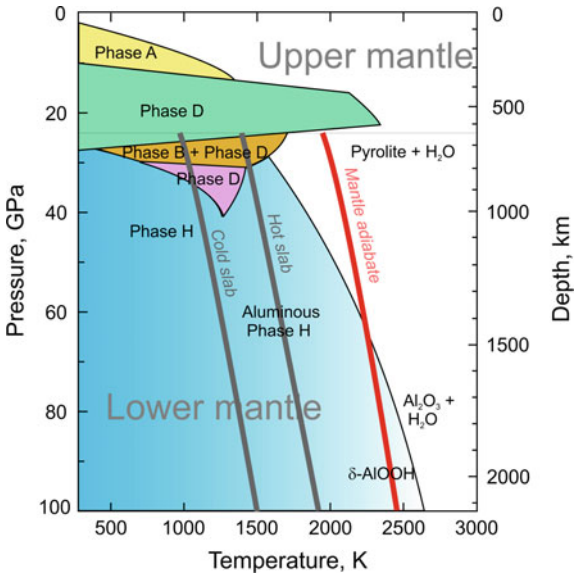

Fig. 5.17 Phase diagram for dense hydrous magnesium silicates in the lower mantle. Temperature profiles in slabs after Kirby et al. (1996). Mantle adiabate after Katsura et al. (2010). Modified after Nishi et al. (2014). Used with a permission of the Nature Geoscience

Bridgmanite in equilibrium with phases D and H has a relatively low Al concentration, and Al partitions preferentially into the hydrous phases (Walter et al. 2015).

The stability of all DHMS phases that are expected to be major inventories of water in subducting slabs are summarized in Fig. 5.17. Phase H in this composition is formed by the reaction of Phase D and periclase, which is assumed to occur at the same pressure as the reaction of Phase D and brucite, although this boundary could be shifted towards higher pressures, defined by the reaction from Phase D to Phase H plus stishovite (Nishi et al. 2014).

High-pressure aluminium-rich phases D and H are more likely to exist in the mafic association because the ultramafic association does not contain enough Al to make these phases stable in the lower-mantle conditions. Phases D and H can survive only in cold subducting slabs because, along an adiabatic geotherm, solid hydrous silicates are not stable. However, to date, none of the DHMS phases were identified in the natural environment.

5.7 Conclusions

The mafic association plays a less important role in the lower mantle compared with the ultramafic one. Firstly, it is much rarer because of the relatively small volume of subducted lithospheric slabs within the lower mantle. Secondly, the structural changes are not so noticeable compared with that in the ultramafic association. For example, a possible NAL to CF phase transition, accompanied by an increase in density, bulk modulus and share wave anisotropy, could be seismically detectable.

However, it is compensated for, in the bulk slab composition, by the faster sound velocity of SiO_2 and its high-pressure polymorphic phase(s). The transitions may be observed only locally within subducting slabs. This means that the mafic association does not play a major role in the general structure of the lower mantle. On the other hand, subducting slabs may cause local seismic anomalies and deliver elements such as Si, Al and water to the deep mantle, forming local water reservoirs within the lower mantle. This may result in local seismic and chemical heterogeneities that can influence deep-mantle geodynamic processes.

References

Andrault, D., Pesce, G., Bouhifd, M. A., Bolfan-Casanova, N., Hénot, J.-M., & Mezouar, M. (2014). Melting of subducted basalt at the core-mantle boundary. *Science, 344*(6186), 892–895.

Akaogi, M. (2007). Phase transitions of minerals in the transition zone and upper part of the lower mantle. In E. Ohtani (Ed.), *Advances in high-pressure mineralogy* (pp. 1–13). Geological Society of America Special Paper 421.

Akaogi, M., Hamada, Y., Suzuki, T., Kobayashi, M., & Okada, M. (1999). High pressure transitions in the system $MgAl_2O_4$–$CaAl_2O_4$: A new hexagonal aluminous phase with implication for the lower mantle. *Physics of the Earth and Planetary Interiors, 115,* 67–77.

Bindi, L., Nishi, M., & Irifune, T. (2015). Partition of Al between phase D and phase H at high pressure: Results from a simultaneous structure refinement of the two phases coexisting in a unique grain. *American Mineralogist, 100,* 1637–1640. doi:10.2138/am-2015-5327

Bindi, L., Nishi, M., Tsuchiya, J., & Irifune, T. (2014). Crystal chemistry of dense hydrous magnesium silicates: The structure of phase H, $MgSiH_2O_4$ synthesized at 45 GPa and 10001000 °C. *American Mineralogist, 99,* 1802–1805. doi:10.2138/am.2014.4994

Boffa Ballaran, T., Frost, D. J., Miyajima, N., & Heidelbach, F. (2010). The structure of a super-aluminous version of the dense hydrous-magnesium silicate phase D. *American Mineralogist, 95,* 1113–1116.

Bolfan-Casanova, N., Andrault, D., Amiguet, E., & Guignot, N. (2009). Equation of state and post-stishovite transformation of Al-bearing silica up to 100 GPa and 3000 K. *Physics of the Earth and Planetary Interiors*, *174*, 70–77. doi:10.1016/j.pepi.2008.06.024

Chang, Y. Y., Jacobsen, S. D., Lin, J. F., Bina, C. R., Thomas, S.-M., Wu, J., et al. (2013). Spin transition of Fe^{3+} in Al-bearing dense hydrous magnesium silicate phase D: An alternative explanation for small-scale seismic scatterers in the mid-lower mantle. *Earth and Planetary Science Letters, 382,* 1–9.

Chen, M., Shu, J., Xie, X., & Mao, H.-K. (2003). Natural $CaTi_2O_4$-structured $FeCr_2O_4$ polymorph in the Suizhou meteorite and its significance in mantle mineralogy. *Geochimica et Cosmochimica Acta, 67,* 3937–3942.

Chung, J. I., & Kagi, H. (2002). High concentration of water in stishovite in the MORB system. *Geophysical Research Letters, 29*(21), 2020. doi:10.1029/2002GL015579

Churakov, S. V., & Wunder, B. (2004). Ab-initio calculations of the proton location in topaz-OH, $Al_2SiO_4(OH)_2$. *Physics and Chemistry of Minerals, 31,* 131–141.

Dai, L., Kudo, Y., Hirose, K., Murakami, M., Asahara, Y., Ozawa, H., et al. (2013). Sound velocities of $Na_{0.4}Mg_{0.6}Al_{1.6}Si_{0.4}O_4$ NAL and CF phases to 73 GPa determined by Brillouin scattering method. *Physics and Chemistry of Minerals, 40,* 195–201.

Davies, R. M., Griffin, W. L., O'Reilly, S. Y., & Doyle, B. J. (2004). Mineral inclusions and geochemical characteristics of microdiamonds from the DO27, A154, A21, A418, DO18, DD17 and Ranch Lake kimberlites at Lac de Gras, Slave Craton, Canada. *Lithos, 77*(1–4), 39–55.

Decker, B. F., & Kasper, J. S. (1957). The structure of calcium ferrite. *Acta Crystallographica Sect B Structure Science, 42,* 229–236.

Egglton, R. A., Boland, J. N., & Ringwood, A. E. (1978). High pressure synthesis of a new aluminum silicate: $Al_5Si_5O_{17}(OH)$. *Geochemical Journal, 12,* 191–194.

Finkelstein, G., Dera, P., Jahn, S., Oganov, A. R., Holl, C. M., Meng, Y., et al. (2014). Phase transitions and equation of state of forsterite to 90 GPa from single-crystal X-ray diffraction and molecular modeling. *American Mineralogist, 99*(1), 35–43. doi:10.2138/am.2014.4526

Frost, D. J. (1999). The stability of dense hydrous magnesium silicates in Earth's transition zone and lower mantle. In Y. Fei, C. M. Bertka, & B. O. Mysen (Eds.), *Mantle petrology: Field observations and high pressure experimentation: A tribute to Francis R. (Joe) Boyd* (pp. 283–296). The Geochemical Society Special Publication No. 6.

Frost, D. J., & Fei, Y. (1998). Stability of phase D at high pressure and high temperature. *Journal of Geophysical Research, 103B,* 7463–7474.

Frost, D. J., & Fei, Y. (1999). Static compression of the hydrous magnesium silicate phase D to 30 GPa at room temperature. *Physics and Chemistry of Minerals, 26,* 415–418.

Fukuyama, K., Ohtani, E., Shibazaki, Y., Kagi, H., & Suzuki, A. (2017). Stability field of phase Egg, $AlSi_3OH$ at high pressure and high temperature: possible water reservoir in mantle transition zone. *Journal of Mineralogical and Petrological Sciences, 112*, 31–35. doi:10.2645/jmps.160719e

Funamori, N., Jealoz, R., Miyajima, N., & Fujino, K. (2000). Mineral assemblages of basalt in the lower mantle. *Journal of Geophysical Research, 105*(B11), 26037–26043.

Ganskow, G., & Langenhorst, F. (2014). Stability and crystal chemistry of iron-bearing dense hydrous magnesium silicates. *Chemie der Erde, 74,* 489–496.

Gasparik, T., Tripathi, A., & Parise, J. B. (2000). Structure of a new Al-rich phase, [K, Na]0.9[Mg, Fe]2[Mg, Fe, Al, Si]6O12, synthesized at 24 GPa. *American Mineralogist, 85,* 613–618.

Gautron L., Fitz Gerald J. D., Kesson S. E., Eggleton R. A., & Irifune, T. (1997). Hexagonal Ba-ferrite: A good model for the crystal structure of a new high-pressure phase $CaAl_4Si_2O_{11}$? *Physics of the Earth and Planetary Interiors, 102*, 223–229.

Gautron, L., Kesson, S. E., & Hibberson, W. O. (1996). Phase relations for $CaAI_2Si_2O_8$ (anorthite composition) in the system CaO–$A1_2O_3$–SiO_2 at 14 GPa. *Physics of the Earth and Planetary Interiors, 97,* 71–81.

Ghosh, S., & Schmidt, M. W. (2014). Melting of phase D in the lower mantle and implications for recycling and storage of H_2O in the deep mantle. *Geochimica et Cosmochimica Acta, 145,* 72–88.

Gleason, A. E., Jeanloz, R., & Kunz, M. (2008). Pressure-temperature stability stud-ies of FeOOH using X-ray diffraction. *American Mineralogist, 93,* 1882–1885.

Gleason, A. E., Quiroga, C. E., Suzuki, A., Pentcheva, R., & Mao, W. L. (2013). Symmetrization driven spin transition in ε-FeOOH at high pressure. *Earth and Planetary Science Letters, 379,* 49–55. doi:10.1016/j.epsl.2013.08.012

Guignot, N., & Andrault, D. (2004). Equations of state of Na–K–Al host phases and implications for MORB density in the lower mantle. *Physics of the Earth and Planetary Interiors, 143–144,* 107–128.

Hayman, P. C., Kopylova, M. G., & Kaminsky, F. V. (2005). Lower mantle diamonds from Rio Soriso (Juina, Brazil). *Contributions to Mineralogy and Petrology, 149*(4), 430–445.

Hirose, K., & Fei, Y. (2002). Subsolidus and melting phase relations of basaltic composition in the uppermost lower mantle. *Geochimica et Cosmochimica Acta, 66,* 2099–2108.

Hirose, K., Fei, Y., Ma, Y., & Mao, H.-K. (1999). The fate of subducted basaltic crust in the Earth's lower mantle. *Nature, 397*(6714), 53–56.

Hirose, K., Takafuji, N., Sata, N., & Ohishi, Y. (2005). Phase transition and density of subducted MORB crust in the lower mantle. *Earth and Planetary Science Letters, 237,* 239–251.

Hushur, A., Manghnani, M. H., Smyth, J. R., Williams, Q., Hellebrand, E., Lonappan, D., et al. (2011). Hydrogen bond symmetrization and equation of state of phase D. *Journal Geophysical Research, 116,* B06203. doi:10.1029/2010JB008087

Hutchison, M. T. (1997). *Constitution of the deep transition zone and lower mantle shown by diamonds and their inclusions*. Unpublished PhD Thesis. University of Edinburgh, UK. Vol. 1, 340 pp., Vol. 2 (Tables and Appendices), 306 pp.

Imada, S., Hirose, K., & Ohishi, Y. (2011). Stabilities of NAL and Ca-ferrite-type phases on the join $NaAlSiO_4$–$MgAl_2O_4$ at high pressure. *Physics and Chemistry of Minerals, 38,* 557–560. doi:10.1007/s00269-011-0427-2

Inoue, T., Wada, T., Sasaki, R., & Yurimoto, H. (2010). Water partitioning in the Earth's mantle. *Physics of the Earth and Planetary Interiors, 183,* 245–251.

Irifune, T., Fujino, K., & Ohtani, E. (1991). A new high-pressure form of $MgAl_2O_4$. *Nature, 349* (6308), 409–411. doi:10.1038/349409a0

Irifune, T., & Ringwood, A. E. (1993). Phase transformations in subducted oceanic crust and buoyancy relationships at depths of 600–800 km in the mantle. *Earth and Planetary Science Letters, 117*(1–2), 101–110.

Irifune, T., Ringwood, A. E., & Hibberson, W. O. (1994). Subduction of continental crust and terrigenous and pelagic sediments: An experimental study. *Earth and Planetary Science Letters, 126,* 351–368.

Kaminsky, F. V., Wirth, R., & Schreiber, A. (2015). A microinclusion of lower-mantle rock and some other lower-mantle inclusions in diamond. *Canadian Mineralogist, 53*(1), 83–104. doi:10.3749/canmin.1400070

Kaminsky, F. V., Zakharchenko, O. D., Davies, R., Griffin, W. L., Khachatryan-Blinova, G. K., & Shiryaev, A. A. (2001). Superdeep diamonds from the Juina area, Mato Grosso State, Brazil. *Contributions to Mineralogy and Petrology, 140*(6), 734–753.

Kanzaki, M. (1989). High pressure phase relations in the system $MgO–SiO_2–H_2O$. *Eos, Transactions American Geophysical Union, 70*(15), 508.

Kanzaki, M. (1991). Stability of hydrous magnesium silicates in the mantle transition zone. *Physics of the Earth and Planetary Interiors, 66,* 307–312.

Kanzaki, M. (2010). Crystal structure of a new high-pressure polymorph of topaz-OH. *American Mineralogist, 95,* 1349–1352. doi:10.2138/am.2010.3555

Kato, C., Hirose, K., Komabayashi, T., Ozawa, H., & Ohishi, Y. (2013). NAL phase in K-rich portions of the lower mantle. *Geophysical Research Letters, 40,* 5085–5088. doi:10.1002/grl.50966

Katsura, T., Yoneda, A., Yamazaki, D., Yoshino, T., & Ito, E. (2010). Adiabatic temperature profile in the mantle. *Physics of the Earth and Planetary Interiors, 183,* 212–218. doi:10.1016/j.pepi.2010.07.001

Kawai, K., & Tsuchiya, T. (2012) Phase stability and elastic properties of the NAL and CF phases in the $NaMg_2Al_5SiO_{12}$ system from first principles. *American Mineralorist, 97*, 305–314. DPI: 10.2138/am.2012.3915

Kesson, S. E., Fitz Gerald, J. D., & Shelley, J. M. (1994). Mineral chemistry and density of subducted basaltic crust at lower mantle pressures. *Nature, 372,* 767–769.

Kirby, S. H., Stein, S., Okal, E. A., & Rubie, D. C. (1996). Metastable mantle phase transformations and deep earthquakes in subducting oceanic lithosphere. *Reviews of Geophysics, 34*(2), 261–306.

Kojitani, H., Hisatomi, R., & Akaogi, M. (2007). High-pressure phase relations and crystal chemistry of calcium ferrite-type solid solutions in the system $MgAl_2O_4–Mg_2SiO_4$. *American Mineralogist, 92,* 1112–1118.

Kojitani, H., Iwabuchi, T., Kobayashi, M., Miura, H., & Akaogi, M. (2011). Structure refinement of high-pressure hexagonal aluminous phases $K_{1.00}Mg_{2.00}Al_{4.80}Si_{1.15}O_{12}$ and $Na_{1.04}Mg_{1.88}Al_{4.64}Si_{1.32}O_{12}$. *American Mineralogist, 96*(9), 1248–1253. doi:10.2138/Am.2011.3638

Komatsu, K., Kuribayashi, T., Sano, A., Ohtani, E., & KudohY. (2006). Redetermination of the high-pressure modification of AlOOH from single-crystal synchrotron data. *Acta Crystallograph Sect E 62*(11), i216–i218, doi:10.1107/S160053680603916X

Komatsu, K., Sano-Furukawa, A., & Kagi, H. (2011). Effects of Mg and Si ions on the symmetry of δ -AlOOH. *Physics and Chemistry of Minerals, 38*(9), 727–733.

Kudoh, Y., Finger, L. W., Hazen, R. M., Prewitt, C. T., Kanzaki, M., & Veblen, D. R. (1993). Phase E: A high pressure hydrous silicate with unique crystal chemistry. *Physics and Chemistry of Minerals, 19,* 357–360.

Kudoh, Y., Kuribayashi, T., Suzuki, A., Ohtani, E., & Kamada, T. (2004). Space group and hydrogen sites of δ-AlOOH and implications for a hypothetical high-pressure form of $Mg(OH)_2$. *Physics and Chemistry of Minerals, 31,* 360–364.

Kudoh, Y., Nagase, T., Mizohata, H., Ohtani, E., Sasaki, S., M. Tanaka, M. (1997) Structure and crystal chemistry of phase G, a new hydrous magnesium silicate synthesized at 22 GPa and 1050 °C. *Geophysical Research Letters, 24*, 1051–1054.

Kudoh, Y., Nagase, T., Sasaki, S., Tanaka, M., & Kanzaki, M. (1995). Phase F, a new hydrous magnesium silicate synthesized at 1000 °C and 17 GPa: Crystal structure and estimated bulk modulus. *Physics and Chemistry of Minerals, 22,* 295–299.

Kurashina, T., Hirose, K., Ono, S., Sata, N., & Ohishi, Y. (2004). Phase transition in Al-bearing $CaSiO_3$ perovskite: Implications for seismic discontinuities in the lower mantle. *Physics of the Earth and Planetary Interiors, 145,* 67–74.

Kuribayashi, T., Sano-Furukawa, A., & Nagase, T. (2013). Observation of pressure-induced phase transition of δ-AlOOH by using single-crystal synchrotron X-ray diffraction method. *Physics and Chemistry Minerals, 41*(4), 303–312. doi:10.1007/s00269-013-0649-6

Lakshtanov, D. L., Sinogeikin, S. V., Konstantin D. Litasov, K. D., Vitali B. Prakapenka, V. B., Hellwig, H., et al. (2007). The post-stishovite phase transition in hydrous Al-bearing SiO_2 in the lower mantle of the Earth. *Proceedings of the National Academy of Sciences of the USA 104*, 13588–13590.

Li, S., Ahuja, R., & Johansson, B. (2006). The elastic and optical properties of the high-pressure hydrous phase δ-AlOOH. *Solid State Communications, 137*(1–2), 101–106. doi:10.1016/j.ssc.2005.08.031

Lin, J.-F., Speciale, S., Mao, Z., & Marquardt, H. (2013). Effects of the electronic spin transitions of iron in lower mantle minerals: implications for deep mantle geophysics and geochemistry. *Reviews of Geophysics, 51*(2), 244–275.

Litasov, K. D., Kagi, H., Shatskiy, A., Ohtani, E., Lakshtanov, D. L., Bass, J. D., et al. (2007a). High hydrogen solubility in Al-rich stishovite and water transport in the lower mantle. *Earth and Planetary Science Letters, 262*(2007), 620–634. doi:10.1016/j.epsl.2007.08.015

Litasov, K. D., & Ohtani, E. (2005). Phase relations in hydrous MORB at 18–28 GPa: Implications for heterogeneity of the lower mantle. *Physics of the Earth and Planetary Interiors, 150,* 239–263. doi:10.1016/j.pepi.2004.10.010

Litasov, K. D., & Ohtani, E. (2007). Effect of water on the phase relations in Earth's mantle and deep water cycle. In E. Ohtani (Ed.), *Advances in High-pressure Mineralogy* (pp. 115–156). Geological Society of America.

Litasov, K. D., Ohtani, E., Nishihara, Y., Suzuki, A., & Funakoshi, K. (2008). Thermal equation of state of Al- and Fe-bearing phase D. *Journal Geophysical Research, 113,* B08205. doi:10.1029/2007JB004937

Litasov, K. D., Ohtani, E., Suzuki, A., & Funakoshi, K. (2007b). The compressibility of Fe- and Al-bearing phase D to 30 GPa. *Physics and Chemistry of Minerals, 34,* 159–167.

Litasov, K., Ohtani, E., Suzuki, A., & Kawazoe, T. (2004). Absence of density crossover between basalt and peridotite in the cold slabs passing through 660 km discontinuity. *Geophysical Research Letters, 31,* L24607. doi:10.1029/2004GL021306

Liu, L. (1977). High pressure $NaAlSiO_4$: The first silicate calcium ferrite isotype. *Geophysical Reseach Letters, 4*(5), 183–186. doi:10.1029/GL004i005p00183

Liu, L.-G. (1986). Phase transformations in serpentine at high pressures and temperatures and implications for subducting lithosphere. *Physics of the Earth and Planetary Interiors, 42,* 255–262.

Liu, L.-G. (1987). Effects of H_2O on the phase behavior of the forsterite-enstatite system at high pressures and temperatures and implications for the Earth. *Physics of the Earth and Planetary Interiors, 49,* 142–167.

Mainprice, D., Le Page, Y., Rodgers, J., & Jouanna, P. (2007). Predicted elastic properties of the hydrous D phase at mantle pressures: Implications for the anisotropy of subducted slabs near 670-km discontinuity and in the lower mantle. *Earth Planetary Science Letters, 259*(3–4), 283–296. doi:10.1016/j.epsl.2007.04.053

Mashino, I., Murakami, M., & Ohtani, E. (2016). Sound velocities of δ-AlOOH up to core-mantle boundary pressures with implications for the seismic anomalies in the deep mantle. *Journal of Geophysical Research: Solid Earth, 121,* 595–609. doi:10.1002/2015JB012477

Miura, H., Hamada, Y., Suzuki, T., Akaogi, M., Miyajima, N., & Fujino, K. (2000). Crystal structure of $CaMg_2Al_6O_{12}$, a new Al-rich high pressure form. *American Mineralogist, 85,* 1799–1803.

Miyajima, N., Fujino, K., Funamori, N., Kondo, T., & Yagi, T. (1999). Garnet–perovskite transformation under conditions of the Earth's lower mantle: An analytical transmission electron microscopy study. *Physics of the Earth and Planetary Interiors, 116,* 117–131.

Miyajima, N., Yagi, T., Hirose, K., Kondo, T., Fujino, K., & Miura, H. (2001). Potential host phase of aluminum and potassium in the Earth's lower mantle. *American Mineralogist, 86,* 740–746.

Mookherjee, M., Karki, B. B., Stixrude, L., Lithgow-Bertelloni, C. (2012). Energetics, equation of state, and elasticity of NAL phase: Potential host for alkali and aluminum in the lower mantle. *Geophysical Research Letters 39*, LI9306. DOI 10.1029/2012GL053682

Mookherjee, M., Tsuchiya, J., & Hariharan, A. (2016). Crystal structure, equation of state, and elasticity of hydrous aluminosilicate phase, topaz-OH ($Al_2SiO_4(OH)_2$) at high pressures. *Physics of the Earth and Planetary Interiors, 251,* 24–35. doi:10.1016/j.pepi.2015.11.006

Nishi, M., Irifune, T., Tsuchiya, J., Tange, Y., Nishihara, Y., Fujino, K., et al. (2014). Stability of hydrous silicate at high pressures and water transport to the deep lower mantle. *Nature Geoscience, 7*(3), 224–227.

Nishihara, Y., & Matsukage, K. N. (2016). Iron-titanium oxyhydroxides as water carriers in the Earth's deep mantle. *American Mineralogist, 101,* 919–927.

Northrup, P. A., Leinenweber, K., & Parise, J. B. (1994). The location of H in the high-pressure synthetic $Al_2SiO_4(OH)_2$ topaz analogue. *American Mineralogist, 79,* 401–404.

Ohira, I., Ohtania, E., Sakaia, T., Miyahara, M., Hirao, N., Ohishi, Y., et al. (2014). Stability of a hydrous δ-phase, AlOOH–$MgSiO_2(OH)_2$, and a mechanism for water transport into the base of lower mantle. *Earth and Planetary Science Letters, 401,* 12–17. doi:10.1016/j.epsl.2014.05.059

Ohtani, E., Amaike, Y., Kamada, S., Sakamaki, T., & Hirao, N. (2014). Stability of hydrous phase H $MgSiO_4H_2$ under lower mantle conditions. *Geophysical Research Letters, 41*(23), 8283–8287. doi:10.1002/2014GL061690

Ohtani, E., Litasov, K., Hosoya, T., Kubo, T., & Kondo, T. (2004). Water transport into the deep mantle and formation of a hydrous transition zone. *Physics of the Earth and Planetary Interiors, 143,* 255–269.

Ohtani, E., Litasov, K., Suzuki, A., & Kondo, T. (2001a). Stability field of new hydrous phase, δ -AlOOH, with implications for water transport into the deep mantle. *Geophysical Research Letters, 28,* 3991–3993.

Ohtani, E., Mitzobata, H., Kudoh, Y., & Nagase, T. (1997). A new hydrous silicate, a water reservoir, in the upper part of the lower mantle. *Geophysical Research Letters, 24,* 1047–1050.

Ohtani, E., Toma, M., Litasov, K., Kubo, T., & Suzuki, A. (2001b). Stability of dense hydrous magnesium silicate phases and water storage capacity in the transition zone and lower mantle. *Physics of the Earth and Planetary Interiors, 124,* 105–117.

Ono, S. (1999). High temperature stability of phase "Egg", $AlSiO_3(OH)$. *Contributions to Mineralogy and Petrology, 137,* 83–89.

Ono, A., Akaogi, M., Kojitani, H., Yamashita, K., & Kobayashi, M. (2009). High-pressure phase relations and thermodynamic properties of hexagonal aluminous phase and calcium–ferrite phase in the systems $NaAlSiO_4$–$MgAl_2O_4$ and $CaAl_2O_4$–$MgAl_2O_4$. *Physics of the Earth and Planetary Interiors, 174,* 39–49.

Ono, S., Ito, E., & Katsura, T. (2001). Mineralogy of subducted basaltic crust (MORB) from 25 to 37 GPa, and chemical heterogeneity of the lower mantle. *Earth and Planetary Science Letters, 190,* 57–63.

Otte, K., Pentcheva, R., Schmahl, W. W., & Rustad, J. R. (2009). Pressure-induced structural and electronic transitions in FeOOH from first principles. *Physical Review B, 80,* 205116. doi:10.1103/PhysRevB.80.205116

Pamato, M. G., Kurnosov, A., Boffa Ballaran, T., Trots, D.M., Caracas, R., & Frost, D. J. (2014). Hexagonal $Na_{0.41}[Na_{0.125}Mg_{0.79}Al_{0.085}]_2[Al_{0.79}Si_{0.21}]_6O_{12}$ (NAL phase): Crystal structure refinement and elasticity. *American Mineralogist 99*(8–9), 1562–1569.

Pamato, M. G., Myhill, R., Ballaran, T. B., Frost, D. J., Heidelbach, F., & Miyajima, N. (2015). Lower-mantle water reservoir implied by the extreme stability of a hydrous aluminosilicate. *Nature Geoscience, 8*(1), 75–79.

Panero, W.R., & Caracas, R. (2017). Stability of phase H in the $MgSiO_4H_2$–AlOOH–SiO_2 system. *Earth and Planetary Science Letters, 463*, 171–177. doi:10.1016/j.epsl.2017.01.033

Panero, W. R., & Stixrude, L. P. (2004). Hydrogen incorporation in stishovite at high pressure and symmetric bonding in δ-AlOOH. *Earth Planetary Science Letters, 221,* 421–431.

Prewitt, C. T., & Parise, J. B. (2000). Hydrous phases and hydrogen bonding at high pressure. In R. M. Hazen & R. T. Downs (Eds.), *High-temperature and high-pressure crystal chemistry* (Vol. 41, pp. 309–333). Virginia: Reviews in Mineralogy and Geochemistry, Mineralogical Society of America, Chantilly.

Reagan, M. M., Gleason, A. E., Daemen, L., Xiao, Y., & Mao, W. L. (2016). High-pressure behavior of the polymorphs of FeOOH. *American Mineralogist, 101,* 1483–1488. doi:10.2138/am-2016-5449

Reid, A. F., & Ringwood, A. E. (1969). Newly observed high pressure transformations in Mn_3O_4, $CaAl_2O_4$, and $ZrSiO_4$. *Earth and Planetary Science Letters, 6,* 205–208. doi:10.1016/0012-821X(69)90091-0

Ricolleau, A., Perrillat, J.-P., Fiquet, G., Daniel, I., Matas, J., Addad, A., et al. (2010). Phase relations and equation of state of a natural MORB: Implications for the density profile of subducted oceanic crust in the Earth's lower mantle. *Journal Geophysical Research, 115,* B08202. doi:10.1029/2009JB006709

Ringwood, A. E., & Major, A. (1967). High-pressure reconnaissance investigations in the system Mg_2SiO_4–MgO–H_2O. *Earth and Planetary Science Letters, 2,* 130–133.

Rosa, A. D., Mezouar, M., Garbarino, G., Bouvier, P., Ghosh, S., Rohrbach, A., et al. (2013a). Single-crystal equation of state of phase D to lower mantle pressures and the effect of hydration on the buoyancy of deep subducted slabs. *Journal of Geophysical Research: Solid Earth, 118* (12), 6124–6133. doi:10.1002/2013JB010060

Rosa, A. D., Sanchez-Valle, C., & Ghosh, S. (2012). Elasticity of phase D and implication for the degree of hydration of deep subducted slabs. *Geophysical Reseach Letters, 39,* L06304. doi:10.1029/2012GL050927

Rosa, A. D., Sanchez-Valle, C., Nisr, C., Evans, S. R., Debord, R., & Merkel, S. (2013b). Shear wave anisotropy in textured phase D and constraints on deep water recycling in subduction zones. *Earth Planetary Science Letters, 377–378,* 13–22.

Sano, A., Ohtani, E., Kondo, T., Hirao, N., Sakai, T., Sata, N., et al. (2008). Aluminous hydrous mineral δ-AlOOH as a carrier of hydrogen into the core-mantle boundary. *Geophysical Reseach Letters, 35,* L03303.

Sano, A., Ohtani, E., Kubo, T., & Finakoshi, K. (2004). In situ X-ray observation of decomposition of hydrous aluminum silicate $AlSiO_3OH$ and aluminum oxide hydroxide δ-AlOOH at high pressure and temperature. *Journal of Physics and Chemistry of Solids, 65,* 1547–1554.

Sano-Furukawa, A., Komatsu, K., Vanpeteghem, C. B., & Ohtani, E. (2008). Neutron diffraction study of δ-AlOOD at high pressure and its implication for symmetrization of the hydrogen bond. *American Mineralogist, 93*(10), 1558–1567. doi:10.2138/am.2008.2849

Schmidt, M. W. (1995). Lawsonite: Upper pressure stability and formation of higher density hydrous phases. *American Mineralogist, 80,* 1286–1292.

Schmidt, M. W., Finger, L. W., Ross, R. J., & Dinnebier, R. E. (1998). Synthesis, crystal structure, and phase relations of $AlSiO_3OH$, a high-pressure hydrous phase. *American Mineralogist, 83* (7–8), 881–888.

Shieh, S. R., Duffy, T. S., Liu, Z., & Ohtani, E. (2009). Highpressure infrared spectroscopy of the dense hydrous magnesium silicates phase D and phase E. *Physics of the Earth and Planetary Interiors, 175*(3–4), 106–114. doi:10.1016/j.pepi.2009.02.002

Shieh, S. R., Mao, H. K., Hemley, R. J., & Ming, L. C. (1998). Decomposition of phase D in the lower mantle and the fate of dense hydrous silicates in subducting slabs. *Earth and Planetary Science Letters, 159,* 13–23.

Shieh, S. R., Mao, H.-K., Hemley, R. J., & Ming, L. C. (2000). In situ X-ray diffraction studies of dense hydrous magnesium silicates at mantle conditions. *Earth and Planetary Science Letters, 177,* 69–80.

Shinmei, T., Irifune, T., Tsuchiya, J., & Funakoshi, K.-I. (2008). Phase transition and compression behavior of phase D up to 46 GPa using multi-anvil apparatus with sintered diamond anvils. *High Pressure Research, 28*(3), 363–373. doi:10.1080/08957950802246514

Stachel, T., Harris, J. W., Brey, G. P., & Joswig, W. (2000). Kankan diamonds (Guinea) II: lower mantle inclusion parageneses. *Contributions to Mineralogy and Petrology, 140*(1), 16–27.

Suzuki, A., Ohtani, E., & Kamada, T. (2000). A new hydrous phase δ-AlOOH synthesized at 21 GPa and 1000 °C. *Physics and Chemistry Mineral, 27,* 689–693.

Tappert, R., Foden, J., Stachel, T., Muehlenbachs, K., Tappert, M., & Wills, K. (2009). The diamonds of South Australia. *Lithos, 112S,* 806–821.

Thomson, A. R., Kohn, S. C., Bulanova, G. P., Smith, C. B., Araujo, D., EIMF, et al. (2014). Origin of sub lithospheric diamonds from the Juina 5 kimberlite (Brazil): Constraints from carbon isotopes and inclusion Compositions. Contributions to Mineralogy and Petrology 168, 1081, 29 pp.

Tschauner, O., Ma, Ch., Beckett, J. R., Prescher, C., Prakapenka, V. B., & Rossman, G. R. (2014). Discovery of bridgmanite, the most abundant mineral in Earth, in a shocked meteorite. *Science, 346*(6213), 1100–1102. doi:10.1126/science.1259369

Tsuchiya, J. (2013). First principles prediction of a new high-pressure phase of dense hydrous magnesium silicates in the lower mantle. *Geophysical Research Letters, 40,* 4570–4573. doi:10.1002/grl.50875

Tsuchiya, J., & Tsuchiya, T. (2011). First-principles prediction of a high-pressure hydrous phase of AlOOH. *Physics Review B, 83,* 054115. doi:10.1103/PhysRevB.83.054115

Tsuchiya, J., Tsuchiya, T., & Tsuneyuki, S. (2005). First-principles study of hydrogen bond symmetrization of phase D under high pressure. *American Mineralogist, 90,* 44–49.

Tsuchiya, J., Tsuchiya, T., Tsuneyuki, S., & Yamanaka, T. (2002). First principles calculation of a high-pressure hydrous phase, δ-AIOOH. *Geophysical Research Letters, 29*(19), 1909. doi:10.1029/2002GL015417

Umemoto, K., Kawamura, K., Hirose, K., & Wentzcovitch, R. M. (2016). Post-stishovite transition in hydrous aluminous SiO_2. *Physics of the Earth and Planetary Interiors, 255,* 18–26. doi:10.1016/j.pepi.2016.03.008

Vanpeteghem, C., Ohtani, E., Kondo, T., Takemura, K., & Kikegawa, T. (2003). Compressibility of phase Egg $AlSiO_3OH$: Equation of state and role of water at high pressure. *American Mineralogist, 88*(10), 1408–1411.

Vanpeteghem, C. B., Sano, A., Komatsu, K., Ohtani, E., & Suzuki, A. (2007). Neutron diffraction study of aluminous hydroxide δ-AlOOD. *Physics Chemistry Minerals, 34*(9), 657–661. doi:10.1007/s00269-007-0180-8

Walter, M. J., Kohn, S. C., Araujo, D., Bulanova, G. P., Smith, C. B., Gaillou, E., et al. (2011). Deep mantle cycling of oceanic crust: Evidence from diamonds and their mineral inclusions. *Science, 334,* 54–57.

Walter, M. J., Thomson, A. R., Wang, W., Lord, O. T., Ross, J., McMahon, S. C., et al. (2015). The stability of hydrous silicates in Earth's lower mantle: Experimental constraints from the systems $MgO–SiO_2–H_2O$ and $MgO–Al_2O_3–SiO_2–H_2O$. *Chemical Geology, 418,* 16–29.

Wicks, J. K., & Duffy, T. S. (2016). Crystal structures of minerals in the lower mantle. In H. Terasaki & R. A. Fischer (Eds.), *Deep earth: Physics and chemistry of the lower mantle and core*. *Geophysical Monograph* (Vol. 217, pp. 69–87).

Wirth, R., Vollmer, C., Brenker, F., Matsyuk, S., & Kaminsky, F. (2007). Nanocrystalline hydrous aluminum silicate in superdeep diamonds from Juina (Mato Grosso State, Brazil). *Earth and Planetary Science Letters, 259*(3–4), 384–399.

Wu, X., Wu, Y., Lin, J.-F., Liu, J., Mao, Z., Guo, X., et al. (2016a). Two-stage spin transition of iron in FeAl-bearing phase D at lower mantle. *Journal of Geophysical Research Solid Earth*, *121*(9), 6411–6420. doi:10.1002/2016JB013209

Wu, Y., Wu, X., Lin, J.-F., McCammon, C. A., Xiao, Y., Chow, P., et al. (2016b). Spin transition of ferric iron in the NAL phase: Implications for the seismic heterogeneities of subducted slabs in the lower mantle. *Earth and Planetary Science Letters, 434,* 91–100. doi:10.1016/j.epsl.2015.11.011

Wunder, B., Rubie, D. C., Ross, C. R., II, Medenbach, O., Seifert, F., & Schreyer, W. (1993). Synthesis, stability and properties and of $Al_2SiO_4(OH)_2$: A fully hydrated analogue of topaz. *American Mineralogist, 78,* 285–297.

Xue, X., Kanzaki, M., Fukui, H., Ito, E., & Hashimoto, T. (2006). Cation order and hydrogen bonding of high-pressure phases in the Al_2O_3–SiO_2–H_2O system: An NMR and Raman study. *American Mineralogist, 91,* 850–861. doi:10.2138/am.2006.2064

Xue, X., Kanzaki, M., & Shatskiy, A. (2008). Dense hydrous magnesium silicates, phase D, and superhydrous B: New structural constraints from one- and two-dimensional 29Si and 1H NMR. *American Mineralogist, 93,* 1099–1111.

Yamada, H., Matsui, Y., & Eiji, I. (1983). Crystal–chemical characterization of $NaAlSiO_4$ with the $CaFe_2O_4$ structure. *Mineralogical Magazine, 47,* 177–181.

Yamamoto, K., & Akimoto, S. (1977). The system MgO–SiO_2–H_2O at high pressures and temperatures-stability field for hydroxyl-chondrodite, hydroxyl-clinohumite and 10 -phase. *American Journal of Science, 277,* 288–312.

Yamanaka, T., Uchida, A., & Nakamoto, Y. (2008). Structural transition of post-spinel phases $CaMn_2O_4$, $CaFe_2O_4$, and $CaTi_2O_4$ under high pressures up to 80 GPa. *American Mineralogist, 93*, 1874–1881. doi 10.2138/am.2008.2934

Yang, H., Prewitt, C. T., & Frost, D. J. (1997). Crystal structure of the dense hydrous magnesium silicate, phase D. *American Mineralogist, 82,* 651–654.

Zedgenizov, D. A., Kagi, H., Shatsky, V. S., & Ragozin, A. L. (2014). Local variations of carbon isotope composition in diamonds from Sao-Luis (Brazil): Evidence for heterogenous carbon reservoir in sublithospheric mantle. *Chemical Geology, 240*(1–2), 114–124.

Zedgenizov, D. A., Shatsky, V. S., Panin, A. V., Evtushenko, O. V., Ragozin, A. L., & Kagi, H. (2015). Evidence for phase transitions in mineral inclusions in superdeep diamonds of the Sao Luiz deposit, Brazil. *Russian Geology and Geophysics, 56*(1), 296–305.